

Quantum simulations of SO(5) many-fermion systems using qudits

Marc Illa ^{1,*}, Caroline E. P. Robin ^{2,3,†} and Martin J. Savage ^{1,‡}

¹*InQubator for Quantum Simulation (IQUS), Department of Physics, University of Washington, Seattle, Washington 98195, USA*

²*Fakultät für Physik, Universität Bielefeld, D-33615 Bielefeld, Germany*

³*GSI Helmholtzzentrum für Schwerionenforschung, Planckstraße 1, D-64291 Darmstadt, Germany*



(Received 4 July 2023; revised 31 October 2023; accepted 21 November 2023; published 7 December 2023)

Background: The structure and dynamics of many-body systems are the result of a delicate interplay between underlying interactions. Fermionic pairing, for example, plays a central role in various physical systems, ranging from condensed matter to nuclear systems, where it can lead to collective phenomena such as superconductivity and superfluidity. In atomic nuclei, the interplay between pairing and particle-hole interactions leads to a high degree of complexity and intricate entanglement structures. Despite this apparent complexity, symmetries emerge and manifest themselves in observable regular patterns. These symmetries and their breakings have long been used to determine relevant degrees of freedom and simplify classical descriptions of many-body systems.

Purpose: This work explores the potential utility of quantum computers with arrays of qudits in simulating interacting fermionic systems, when the qudits can naturally map the relevant degrees of freedom determined by an underlying symmetry group.

Method: The Agassi model of fermions interacting via particle-hole and pairing interactions is based on an underlying $so(5)$ algebra. Such systems can intuitively be partitioned into pairs of modes with five basis states, which thus naturally map to arrays of $d = 5$ qudits (qu5its). Classical noiseless simulations of the time evolution of systems with up to twelve qu5its are performed, by implementing quantum circuits that are developed herein, using PYTHON codes invoking Google's CIRQ software. The resource requirements of the qu5it circuits are analyzed and compared with two different mappings to qubit systems: a physics-aware Jordan-Wigner mapping requiring four qubits per mode pair and a state-to-state mapping requiring three qubits per mode pair.

Results: While the dimensionality of Hilbert spaces in mappings to qu5it systems are less than those for the corresponding qubit systems, the number of entangling operations, depending on the available hardware, can either be greater or smaller than for the physics-aware Jordan-Wigner mapping. The state-to-state mapping, while having a smaller Hilbert space than Jordan-Wigner mappings, appears to be the least efficient in gate counts. Further, a previously unknown sign problem has been identified from Trotterization errors in time evolving high-energy excitations.

Conclusions: There appear to be advantages in employing quantum computers with arrays of qudits to perform simulations of many-body dynamics that exploit the role of underlying symmetries, specifically in lowering the required quantum resources and in reducing anticipated errors that take the simulation out of the physical space. If the necessary entangling gates are not directly supported by the hardware, physics-aware mappings to qubits may, however, be advantageous for other aspects.

DOI: [10.1103/PhysRevC.108.064306](https://doi.org/10.1103/PhysRevC.108.064306)

I. INTRODUCTION

Pairing of fermionic particles plays a special role in the structure and dynamics of quantum many-body systems of physical importance in our everyday lives. This phenomenon provides the underlying mechanism responsible for superconductivity and superfluidity [1–3], and it is crucial to the description of exotic materials [4–7], structure, reaction, and decay properties of nuclei [8], and matter at extreme densities [9]. Such systems are typically challenging to simulate

with classical computers due to their fundamentally quantum nature, and the role that entanglement and quantum correlations play in their structure; see, for example, Ref. [10]. From a nuclear physics perspective, there is growing interest in better understanding the entanglement structure of hadrons and nuclei [11–40], with the potential to advance our ability to compute the properties and dynamics of nuclear many-body systems through entanglement reorganization [25,38]. This is driven, in part, by the emergence of early quantum computers and simulators, and their accessibility to domain scientists who, in co-design partnership with quantum information scientists, are progressing toward understanding the capabilities, algorithms, and software required to establish a quantum advantage for scientific applications. The capabilities that quantum computers offer beyond classical computing

*marcilla@uw.edu

†crobin@physik.uni-bielefeld.de

‡mjs5@uw.edu; on leave from the Institute for Nuclear Theory.

are the control of entanglement and coherence, the same elements that limit classical simulations of quantum many-body systems, including those involving fermionic pairing.

Various quantum algorithms aiming at solving fermionic pairing Hamiltonians have been proposed in symmetry-breaking plus restoration frameworks and particle-number preserving approaches at zero [41–45] and finite temperature [46]. In addition to pairing phenomena, nuclei also display important particle-hole correlations. The Agassi model [47], which we have chosen to study in this work, is an exactly solvable model which, in part, reveals the interplay between the pairing force and particle-hole interactions of the monopole-monopole type. This model constitutes an extension of the Lipkin-Meshkov-Glick (LMG) model [48], which was initially formulated in the context of nuclear physics studies. The LMG model can be considered to be a system of spin- $\frac{1}{2}$ particles distributed on a simplex in the presence of a background magnetic field and with equal strength interactions that create and annihilate even numbers of particle-hole pairs. The occupation of each mode is fixed, and particles can be promoted or demoted within a mode by the action of the interactions. The LMG model has also been the subject of a large number of studies in condensed matter, as it was subsequently found to be relevant for describing the Josephson effect [49] and two-mode Bose-Einstein condensates [50]. Further, a more general class of LMG models are known to provide a means to prepare spin-squeezed states [51] through time evolution away from a tensor-product state, of utility in quantum sensing [52–54]. These many features have motivated intense work aiming at investigating the entanglement properties of the LMG model, in particular the entanglement and quantum correlations of the ground state near the phase transitions (see, e.g., Refs. [35,55–61]), as well as the dynamics of entanglement measures [50]. Given that the building blocks of the model are SU(2) spins, it has been the focus of recent studies using currently available simulators and quantum computers to determine ground-state energies using the variational quantum eigensolver (VQE) [62,63], or ADAPT-VQE [64] with different wave-function *Ansätze*. Recently, we have shown [38] that the LMG model can be efficiently implemented throughout much of the Hilbert space via rearrangement of entanglement induced by global SU(2) rotations. The rotation angle can be learned in the VQE process of determining the ground state, with the Hamiltonian learning VQE (HL-VQE) that we introduced in Ref. [38], for a given truncation of the model space. Exponential convergence was demonstrated throughout large fractions of the Hilbert space [38]. Further, recent work used the quantum equation of motion (qEOM) algorithm [65], a modification of VQE, to determine excited states in the LMG model [66].

The importance of pairing in nuclear physics, and other areas, motivated an extension to the LMG model by the inclusion of a pairing term, known as the Agassi model. In this model, pairs of particles from mode pairs can scatter by changing both their states within the mode pair, or can scatter into pairs of unoccupied states in other mode pairs. As a result, this model has a more interesting phase diagram than the LMG model. Specifically, with two dimensionless parameters, this model has a phase diagram that exhibits a

spherical phase, a deformed phase, and a superfluid Bardeen-Cooper-Schrieffer (BCS) phase [67,68]. The nature of the pairing interaction is such that the number of particles is preserved throughout time evolution, and a five-dimensional Hilbert space is required for an even number of particles in two modes, forming the fundamental representation of an SO(5) symmetry in the absence of interactions. Generally speaking, models exhibiting an SO(5) symmetry are ubiquitous in quantum many-body physics; see, e.g., Refs. [5,69].

Having recognized the potential role of future quantum simulations in advancing our understanding of such pairing models and establishing their predictive capabilities, the first pioneering works on simulating the dynamics of the Agassi model for small systems were recently performed [70,71]. In those works, a Jordan-Wigner (JW) mapping was used to simulate systems with two and four modes using one qubit per site to define its occupation, without appealing to their inherent SO(5) symmetries. In the present work, we find advantages in making use of the SO(5) symmetry in mapping pairs of modes (four sites) to five-dimensional qudits (which we call qu5its), to enable more efficient quantum simulations of such systems. While qubits form the quantum registers of many digital quantum computers that are presently available, significant progress is being made toward qudit quantum registers, particularly using superconducting radio frequency (SRF) cavities [72,73], superconducting qudit devices [74–81], nitrogen vacancy (NV) centers in diamond [82–84], and most recently trapped ion quantum computers [85–88]. There are well-known motivations for advancing beyond qubits to qudits, including in computation [89–94], cryptography [95,96], and error correction [97–99]. We expect that early arrays of qu5its will become available in the near future, at which point simulations of the Agassi model can be performed using qu5its. In another arena, the utility of qudit systems in simulating (non-)Abelian lattice gauge theories, including lattice QCD, is being explored (see, e.g., Refs. [100–104]), where the qudits provide a commensurate Hilbert space for each truncated gauge link space. Further, the LMG model, which described the dynamics of systems of coupled spin- $\frac{1}{2}$ particles or spins, simulated with arrays of qubits, has been generalized to systems of coupled spin- d particles or spins simulated with arrays of qudits [105].

We note that the Agassi model, or pairing-plus-monopole model, is one physical interpretation of the $so(5)$ [sp(4)] algebra. As is well known, there are at least two other interpretations of this algebra, which lead to other models of interest for nuclear physics; see, e.g., Refs. [69,106,107]. These include the charge-independent pairing model [108,109] describing like-particle and proton-neutron pairing coupled to total isospin $T = 1$, and the vibration-rotation model in two dimensions. In each of these models the Hamiltonian is described by a subset of the generators of SO(5), and different subalgebras correspond to the limits of the model. Although in this work we restrict ourselves to the Agassi model, the techniques developed here can also be applied to these other interpretations of the SO(5) symmetry group.

This paper is organized as follows. In Sec. II, the main aspects of the Agassi model are reviewed. In Sec. III, quantum circuits for preparing initial states on a qu5it register,

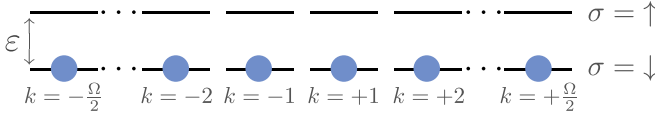


FIG. 1. The lowest-energy noninteracting (0p-0h) configuration of a system of Ω particles in the LMG model.

and for a subsequent Trotterized time evolution [110], are constructed. Results obtained from classical simulations of the time evolution of systems up to 24 modes, using *Mathematica*, *JULIA*, and *PYTHON* code built on CIRQ’s qudit capabilities, are presented. In Sec. IV, the complexity of the quantum circuits for qu5its are compared to those of circuits using mappings onto qubits.

II. THE AGASSI MODEL: LIPKIN-MESHKOV-GLICK HAMILTONIAN, PAIRING INTERACTIONS, AND SO(5) SYMMETRY

In this section, we review the Agassi model, starting from the limit without pairing, which constitutes the LMG model. The low-lying energy spectra of the Agassi model are examined for selected sets of Hamiltonian couplings, given in Table IV, to establish the inputs for quantum simulations with both qubits and qu5its.

A. The Lipkin-Meshkov-Glick model

In its original formulation, the LMG model [48] describes a system of $N = \Omega$ fermions, each distributed on two levels with energy $\pm\epsilon/2$, as shown in Fig. 1. We denote the single-particle states (“sites”) by (k, σ) , where $\sigma = \uparrow, \downarrow$ refers to the upper and lower levels, respectively, and $k = \pm 1, \pm 2, \dots, \pm\Omega/2$ denotes the modes. The Hamiltonian¹ governing the system is

$$\hat{H} = \frac{\epsilon}{2} \sum_k (\hat{c}_{k,\uparrow}^\dagger \hat{c}_{k,\uparrow} - \hat{c}_{k,\downarrow}^\dagger \hat{c}_{k,\downarrow}) - \frac{V}{2} \sum_{k,k'} (\hat{c}_{k,\uparrow}^\dagger \hat{c}_{k',\uparrow}^\dagger \hat{c}_{k',\downarrow} \hat{c}_{k,\downarrow} + \hat{c}_{k,\downarrow}^\dagger \hat{c}_{k',\downarrow}^\dagger \hat{c}_{k',\uparrow} \hat{c}_{k,\uparrow}), \quad (1)$$

where the operators $\hat{c}_{k,\sigma}^\dagger$ and $\hat{c}_{k,\sigma}$ create and destroy a particle in level σ of state k , respectively. The first term accounts for the single-particle energies, while the interaction term scatters particles from the lower to the upper level, or vice versa, within the same modes. Each of the particles interact with equal strength with the others [50,56]. This is illustrated in Fig. 1, which shows the lowest-energy, or “zero-particle–zero-hole” (0p-0h), non-interacting configuration of the system.

The LMG model can be mapped into a system of N interacting spins in a background magnetic field by introducing the

collective spin operators

$$\begin{aligned} \hat{S}_z &= \frac{1}{2} \sum_{k=-\Omega/2}^{\Omega/2} (\hat{c}_{k,\uparrow}^\dagger \hat{c}_{k,\uparrow} - \hat{c}_{k,\downarrow}^\dagger \hat{c}_{k,\downarrow}) = \sum_{k=-\Omega/2}^{\Omega/2} \hat{S}_{k,z}, \\ \hat{S}_+ &= \sum_{k=-\Omega/2}^{\Omega/2} \hat{c}_{k,\uparrow}^\dagger \hat{c}_{k,\downarrow} = \sum_{k=-\Omega/2}^{\Omega/2} \hat{S}_{k,+}, \\ \hat{S}_- &= (\hat{S}_+)^\dagger, \end{aligned} \quad (2)$$

transforming in the adjoint representation of SU(2). The Hamiltonian in Eq. (1) can then be written as

$$\hat{H} = \epsilon \hat{S}_z - \frac{V}{2} (\hat{S}_+^2 + \hat{S}_-^2). \quad (3)$$

B. The Agassi model and SO(5) Symmetry

The Agassi model [47] adds a pairing interaction to the previous LMG model, with a Hamiltonian of the form

$$\hat{H} = \epsilon \hat{S}_z - \frac{V}{2} (\hat{S}_+^2 + \hat{S}_-^2) - g \hat{B}^\dagger \hat{B}. \quad (4)$$

It is convenient to write the collective operators in Eq. (4) in terms of operators acting on pairs of modes $(k, -k)$,

$$\hat{S}_\alpha = \sum_{k=1}^{\Omega/2} \hat{T}_{k,\alpha}, \quad \hat{B} = \sum_{k=1}^{\Omega/2} (\hat{b}_{k,\uparrow} + \hat{b}_{k,\downarrow}), \quad (5)$$

with

$$\begin{aligned} \hat{T}_{k,+} &= \hat{c}_{k,\uparrow}^\dagger \hat{c}_{k,\downarrow} + \hat{c}_{-k,\uparrow}^\dagger \hat{c}_{-k,\downarrow}, & \hat{T}_{k,-} &= \hat{T}_{k,+}^\dagger, \\ \hat{T}_{k,z} &= \frac{1}{2} (\hat{c}_{k,\uparrow}^\dagger \hat{c}_{k,\uparrow} + \hat{c}_{-k,\uparrow}^\dagger \hat{c}_{-k,\uparrow} - \hat{c}_{k,\downarrow}^\dagger \hat{c}_{k,\downarrow} - \hat{c}_{-k,\downarrow}^\dagger \hat{c}_{-k,\downarrow}), \\ \hat{b}_{k,\uparrow} &= \hat{c}_{-k,\uparrow} \hat{c}_{k,\uparrow}, & \hat{b}_{k,\downarrow} &= \hat{c}_{-k,\downarrow} \hat{c}_{k,\downarrow}, \\ \hat{b}_{k,z} &= \frac{1}{\sqrt{2}} (\hat{c}_{-k,\uparrow} \hat{c}_{k,\downarrow} + \hat{c}_{-k,\downarrow} \hat{c}_{k,\uparrow}), \\ \hat{N}_k &= \hat{c}_{k,\uparrow}^\dagger \hat{c}_{k,\uparrow} + \hat{c}_{-k,\uparrow}^\dagger \hat{c}_{-k,\uparrow} + \hat{c}_{k,\downarrow}^\dagger \hat{c}_{k,\downarrow} + \hat{c}_{-k,\downarrow}^\dagger \hat{c}_{-k,\downarrow}, \end{aligned} \quad (6)$$

which, along with $\hat{b}_{k,\uparrow}^\dagger$, $\hat{b}_{k,\downarrow}^\dagger$ and $\hat{b}_{k,z}^\dagger$, constitute a set of ten generators of SO(5) (see Appendix A). The additional pairing term, with coupling constant g , furnishes interactions such as $\hat{c}_{k,\downarrow} \hat{c}_{-k,\downarrow} (\hat{c}_{q,\downarrow} \hat{c}_{-q,\downarrow})^\dagger$ and $\hat{c}_{k,\uparrow} \hat{c}_{-k,\uparrow} (\hat{c}_{k',\downarrow} \hat{c}_{-k',\downarrow})^\dagger$, which, unlike the LMG model, can change the occupation number of a given mode. As in the LMG model, the Agassi model has all modes interacting with equal strength, and hence there is no intrinsic concept of distance.

A five-dimensional set of basis states supporting a wave function on one pair of modes $(k, -k)$ can be defined in terms of single-particle occupation numbers as

$$\begin{aligned} &|n_{k\downarrow}, n_{k\uparrow}, n_{-k\downarrow}, n_{-k\uparrow}\rangle \\ &\in \left\{ |0000\rangle, |1010\rangle, \frac{1}{\sqrt{2}} (|0110\rangle + |1001\rangle), \right. \\ &\quad \left. |0101\rangle, |1111\rangle \right\} \\ &= \{|0\rangle, |1\rangle, |2\rangle, |3\rangle, |4\rangle\}, \end{aligned} \quad (7)$$

¹The LMG Hamiltonian in principle also contains a “swap” term that can lower a particle from (k, \uparrow) to (k, \downarrow) while exciting another from (k', \downarrow) to (k', \uparrow) . We do not include this term as it does not appear in the Agassi model [47].

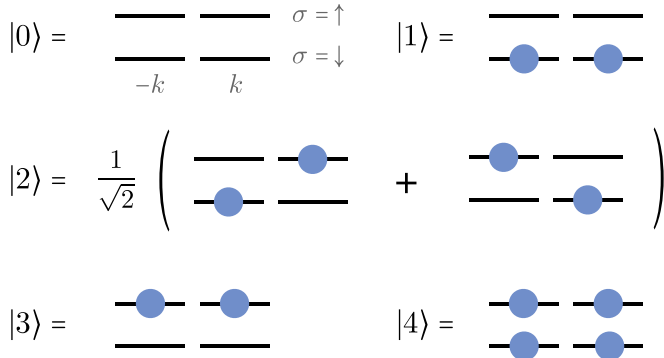


FIG. 2. Basis states for a wave function of one pair of modes $(k, -k)$, as defined in Eq. (7).

which form a fundamental representation of $SO(5)$ generated by the operators in Eq. (6). The basis states in Eq. (7) are schematically represented in Fig. 2. Each of them has a well defined particle number $(0,2,2,2,4)$, pair number $(0,1,0,1,2)$, third component of spin $(0, -1, 0, 1, 0)$, and parity $(1, 1, -1, 1, 1)$.

The phase diagram of the Agassi model is interesting, and has been previously investigated via mean-field calculations of the ground state in the $N = \Omega$ sector; see, for example, Refs. [67,68]. The hierarchies in the parameters ε , V , and g define the three phases of the system: a *symmetric phase*, for which a spherical mean-field description is adapted, and two symmetry-broken phases, a *deformed phase* (parity-broken) and a *superfluid BCS phase*. It has been found helpful to form dimensionless parameters when discussing the structure of the theory:

$$\begin{aligned} \bar{v} &= \frac{(\Omega - 1)V}{\varepsilon}, \\ \bar{g} &= \frac{(\Omega - 1)g}{\varepsilon}, \quad \bar{g}_0 = \bar{g} + \frac{V}{\varepsilon}. \end{aligned} \quad (8)$$

In the large- Ω limit, the mean-field analysis has shown [67] that, for $\bar{v} < 1$ and $\bar{g}_0 < 1$, the system is in the symmetric phase (spherical nonsuperfluid), and the ground state is gapped below the excited states. For $\bar{v} > 1$ and $\bar{g}_0 < \bar{v}$, the system is in a deformed phase, with a doubly degenerate ground state of mixed parity, which is gapped to the excited states. Finally, for $\bar{v} < \bar{g}_0$, $\bar{g}_0 > 1$, the system is in a BCS phase, with degenerate states (having different particle numbers) that are gapped to excited states.

For the small- and modest- Ω systems that are solved exactly in this work, the structures of the systems are found to approach those of the large- Ω limit, modified by finite-size effects. For $\bar{v}, \bar{g}_0 \lesssim 1$, as is the case in the large- Ω limit, the system has an isolated even-parity ground state that is gapped below excited states, with the wave function dominated by a single configuration with all N particles in the lower spin state, $|1\rangle$. For $\bar{v} \gtrsim \bar{g}_0 \gtrsim 1$, there are two low-lying states of opposite parity that are gapped to higher excited states, with wave functions dominated by configurations where the particles occupy states $|1\rangle, |2\rangle, |3\rangle$. Finally, for $\bar{v} \lesssim \bar{g}_0$, $\bar{g}_0 \gtrsim 1$, there are two low-lying states of even parity that are gapped

to excited states, with wave functions dominated by configurations with different particle numbers, where particles occupy states $|0\rangle, |1\rangle, |3\rangle$, and $|4\rangle$. This phase structure has also been investigated in terms of the quantum discord in Ref. [60].

In the quantum simulations performed in the next sections, we select, for demonstrative purposes, the following numerical values of the couplings:

$$\begin{aligned} (\varepsilon, V, g) : \text{set-0} &= (1.0, 0.0, 0.0), \\ &: \text{set-1} = (1.0, 0.5, 0.5), \\ &: \text{set-2} = (1.0, 1.5, 0.5), \\ &: \text{set-3} = (1.0, 0.5, 1.5), \\ &: \text{set-4} = (1.0, 1.5, 1.5). \end{aligned} \quad (9)$$

Set-0 corresponds the noninteracting symmetric case. Set-1, set-3 and set-4, lead to a superfluid phase for $N = \Omega > 2$, while set-2 corresponds to a deformed phase for $N = \Omega > 2$. As mentioned in, e.g., Ref. [70], the case $\Omega = 2$ has only one symmetry-broken phase (see also Sec. III A). In that case, the system is in the symmetry-broken phase with parameters set-2, set-3, and set-4, and at the critical point with set-1. In Table IV of Appendix B we show the lowest-lying energies of systems (specifically, the average energy per mode, $\mathcal{E}_i = E_i/\Omega$) obtained with the aforementioned sets of couplings, for $\Omega = 2, 4, 6, 8$, in different particle-number sectors.

III. QUANTUM SIMULATIONS USING QUSITS ($d = 5$ QUSITS)

In the first pioneering quantum simulation of the Agassi model [70], a JW mapping to qubits was employed to define the occupation of each site in the Hilbert space of a four-site (one-mode-pair) system. This simulation was able to describe a two-particle system evolving throughout the 2^4 dimensional Hilbert space, and was later expanded to four particles using eight qubits [71]. With such a mapping, systems with 2Ω sites, i.e., $\Omega/2$ mode pairs, would be embedded into a $2^{2\Omega}$ dimensional space.

The basis for each pair of modes in Eq. (7) naturally embeds into a five-dimensional ($d = 5$) qudit—a “qu5it.” With the expectation that qudit quantum computers become accessible in the near future, particularly, those that support qu5its, we develop the quantum circuits required for qu5it simulations and compare with equivalent circuits for qubit systems. In developing quantum circuits for state preparation and time evolution, it is most convenient to work with Givens rotations between states within a qu5it, and tensor-products of Givens rotations for entangling operations between qu5its. As the Hamiltonian in Eq. (4) is quadratic in operations between $SO(5)$ irreps, establishing the quantum circuits for systems of one- and two-mode-pair (qu5its) systems is sufficient for generalizing to systems with arbitrary numbers of mode pairs.

Consequently, in this section we present qu5it circuits for the preparation of arbitrary initial states and implementation of their time evolution, for one- and two-mode-pair systems. The generalization to higher number of mode pairs is discussed and implemented in simulators of arrays of qu5its, with comparison to exact time evolution. For the numerical

simulations performed using a qu5it simulator, as well as exact matrix exponentiations, two tensor-product initial states (that can be straightforwardly prepared) are employed. These are

$$\begin{aligned} |\psi(0)\rangle_A &= |1\rangle^{\otimes \Omega/2}, \\ |\psi(0)\rangle_B &= |4\rangle^{\otimes \Omega/4} \otimes |0\rangle^{\otimes \Omega/4}. \end{aligned} \quad (10)$$

Both of these states correspond to half-filled configurations, meaning that the number of particles N equals the number of modes Ω , which equals twice the number of qu5its N_{q5} . State $|\psi(0)\rangle_A$ is the ground state of the noninteracting systems, where all of the particles are in the spin- \downarrow single-particle state. State $|\psi(0)\rangle_B$, on the other hand, is the state in which all of the particles are concentrated into half of the mode pairs only, i.e., they occupy single-particle states (k, σ) with $|k| = \{1, \dots, \Omega/4\}$ and $\sigma = \{\uparrow, \downarrow\}$. $|\psi(0)\rangle_B$ energetically lies far above the noninteracting ground state.

A. One mode pair (one qu5it)

The Hamiltonian for a single mode pair ($\Omega = 2$) in the basis in Eq. (7) is given by

$$\hat{H}_1 = \varepsilon \hat{T}_z - (V + g) \hat{\mathcal{X}}_{13} - g \hat{N}_{\text{pairs}}, \quad (11)$$

where \hat{T}_z is

$$T_z = \begin{pmatrix} 0 & 0 & 0 & 0 & 0 \\ 0 & -1 & 0 & 0 & 0 \\ 0 & 0 & 0 & 0 & 0 \\ 0 & 0 & 0 & 1 & 0 \\ 0 & 0 & 0 & 0 & 0 \end{pmatrix}, \quad (12)$$

\hat{N}_{pairs} is the operator that counts the number of pairs $[(1, \sigma), (-1, \sigma)]$,

$$N_{\text{pairs}} = \begin{pmatrix} 0 & 0 & 0 & 0 & 0 \\ 0 & 1 & 0 & 0 & 0 \\ 0 & 0 & 0 & 0 & 0 \\ 0 & 0 & 0 & 1 & 0 \\ 0 & 0 & 0 & 0 & 2 \end{pmatrix}, \quad (13)$$

and the Givens operator $\hat{\mathcal{X}}_{13}$ is

$$\mathcal{X}_{13} = \begin{pmatrix} 0 & 0 & 0 & 0 & 0 \\ 0 & 0 & 0 & 1 & 0 \\ 0 & 0 & 0 & 0 & 0 \\ 0 & 1 & 0 & 0 & 0 \\ 0 & 0 & 0 & 0 & 0 \end{pmatrix}. \quad (14)$$

The indices of \mathcal{X}_{ij} are defined by the labels of the states in Eq. (7), $i, j, \in \{0, 1, 2, 3, 4\}$.

1. State preparation of one qu5it

Preparing an initial state on a single qu5it is straightforward. Arbitrary transformations among the states of a qu5it can be accomplished with SU(5) unitary operations, with the

associated 24 generators. For the SO(5) transformations relevant for the LMG and Agassi models, this number is reduced to 10. However, to prepare a real wave function from a given initial state of a qu5it, only four parameters are required to establish the five real numbers, one for each state in the Hilbert space, subject to the probability constraint. Therefore, the transformation matrices produced by the Givens operators $\hat{\mathcal{X}}_{01}, \hat{\mathcal{X}}_{12}, \hat{\mathcal{X}}_{23}, \hat{\mathcal{X}}_{34}$, given in Appendix C, or any other spanning set, are sufficient to prepare any real initial state of a qu5it from, say, $|1\rangle$:

$$|\psi\rangle = e^{-i\theta_3 \hat{\mathcal{X}}_{34}} e^{-i\theta_2 \hat{\mathcal{X}}_{23}} e^{-i\theta_1 \hat{\mathcal{X}}_{12}} e^{-i\theta_0 \hat{\mathcal{X}}_{01}} |1\rangle. \quad (15)$$

This same wave function parametrization of the single qu5it can be used in finding the ground-state wave function, using, for instance, VQE [111,112] or variants thereof [65,113–120], by minimizing the ground-state energy with respect to the $\theta_{0,1,2,3}$. The expression in Eq. (15) is a general form for initializing a state, and it can be simplified by utilizing symmetries. The number of particles is preserved in the time evolution of the system, and, as such, if the device can be prepared in a state of the target particle number, then the number of required rotation angles can be reduced. For example, the states $|0\rangle$ and $|4\rangle$ are the ground states of the $N = 0$ and $N = 4$ sectors of one qu5it.

2. Time evolution of one qu5it

As is well known, the time evolution of a state prepared on a qu5it can be evolved forward in time by application of the evolution operator $\hat{U}(t) = e^{-it\hat{H}}$. For the system we are considering, the Hamiltonian is given in Eq. (11), and involves contributions from two diagonal phase operators and one Givens operator, $\hat{\mathcal{X}}_{13}$. This evolution operator can be determined exactly,

$$U(t) = \begin{pmatrix} 1 & 0 & 0 & 0 & 0 \\ 0 & e^{igt}(a(t) + ib(t)) & 0 & ie^{igt}c(t) & 0 \\ 0 & 0 & 1 & 0 & 0 \\ 0 & ie^{igt}c(t) & 0 & e^{igt}(a(t) - ib(t)) & 0 \\ 0 & 0 & 0 & 0 & e^{i2gt} \end{pmatrix}, \quad (16)$$

with

$$\begin{aligned} a(t) &= \cos \alpha t, & b(t) &= \beta \sin \alpha t, & c(t) &= \gamma \sin \alpha t, \\ \alpha &= \sqrt{\varepsilon^2 + (g + V)^2}, & \beta &= \frac{\varepsilon}{\alpha}, & \gamma &= \frac{g + V}{\alpha}. \end{aligned} \quad (17)$$

The exact time evolution of $\langle \hat{S}_z \rangle$ and the amplitude for survival of the ground state of one qu5it, prepared initially in state $|1\rangle$ [corresponding to $|\psi(0)\rangle_A$ in Eq. (10)], and obtained with the parameter sets defined in Eq. (9), are shown in Fig. 3. The Hamiltonian is such that state $|1\rangle$ only couples to state $|3\rangle$ under time evolution, causing the number of pairs to be time independent in the $\Omega = 2$ system. It is clear from Eqs. (11) and (16) that the structure and dynamics of systems on a single mode pair are governed by one dimensionless parameter $(g + V)/\varepsilon$. Such systems thus only present two phases: a symmetric phase for $g + V < \varepsilon$ and a symmetry-broken phase for $g + V > \varepsilon$. The sets of parameters set-2 and set-3 are thus

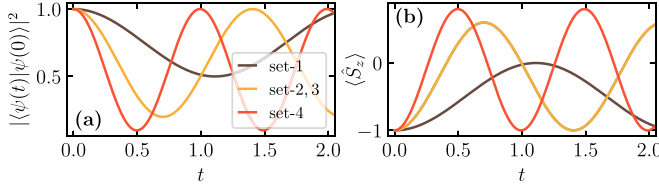


FIG. 3. The exact time dependence of (a) $|\langle\psi(t)|\psi(0)\rangle|^2$ and (b) $\langle\hat{S}_z\rangle$ for a system with $\Omega = 2$ starting in the initial state $|\psi(0)\rangle_A = |1\rangle$, for four sets of couplings, set-1 to set-4, given in Eq. (9).

equivalent, and the set-1 corresponds to the critical point of phase transition.

Trotterization [110] of the evolution operator does not exactly recover the form given in Eq. (16) because, although $[\hat{\mathcal{X}}_{13}, \hat{N}_{\text{pairs}}] = [\hat{T}_z, \hat{N}_{\text{pairs}}] = 0$, the operators $\hat{\mathcal{X}}_{13}$ and \hat{T}_z do not commute. More precisely,

$$[\varepsilon\hat{T}_z - g\hat{N}_{\text{pairs}}, -(g+V)\hat{\mathcal{X}}_{13}] = i2(g+V)\varepsilon\hat{\mathcal{Y}}_{13},$$

$$\mathcal{Y}_{13} = i \begin{pmatrix} 0 & 0 & 0 & 0 & 0 \\ 0 & 0 & 0 & -1 & 0 \\ 0 & 0 & 0 & 0 & 0 \\ 0 & 1 & 0 & 0 & 0 \\ 0 & 0 & 0 & 0 & 0 \end{pmatrix}. \quad (18)$$

As such, there will be Trotter errors in digitized time evolution performed using quantum circuits, for which a leading-order (LO) Trotterization can take the form

$$\hat{U}(t) \simeq [\hat{U}(\Delta t)]^{n_{\text{Trot}}},$$

$$\hat{U}(\Delta t) \simeq e^{i\Delta t(g+V)\hat{\mathcal{X}}_{13}} e^{-i\Delta t\varepsilon\hat{T}_z} e^{i\Delta t g\hat{N}_{\text{pairs}}}, \quad (19)$$

where Δt is the Trotter time step and $n_{\text{Trot}} = t/\Delta t$ is the number of steps.

B. Two mode pairs (two qu5its)

Systems with two or more mode pairs allow for the possibility of moving pairs of particles between modes, and for the possibility of breaking pairs (through the monopole interaction V) while conserving the total number of particles. This introduces a richness that is not present for a single mode pair. Because there is an even number of fermions per mode pair, mappings to systems with more than one qu5it are effectively bosonic, without potential negative signs associated with operators acting on separated qu5its. For two mode pairs ($\Omega = 4$), the Hamiltonian in Eq. (4) reduces to

$$\begin{aligned} \hat{H}_2 = & \varepsilon(\hat{T}_{1,z} + \hat{T}_{2,z}) - V(\hat{T}_{1,+}^2 + \hat{T}_{2,+}^2 + \hat{T}_{1,-}^2 + \hat{T}_{2,-}^2 \\ & + \{\hat{T}_{1,+}, \hat{T}_{2,+}\} + \{\hat{T}_{1,-}, \hat{T}_{2,-}\}) \\ & - g[(\hat{b}_{1,\uparrow} + \hat{b}_{1,\downarrow})^\dagger(\hat{b}_{1,\uparrow} + \hat{b}_{1,\downarrow}) \\ & + (\hat{b}_{2,\uparrow} + \hat{b}_{2,\downarrow})^\dagger(\hat{b}_{2,\uparrow} + \hat{b}_{2,\downarrow}) \\ & + (\hat{b}_{1,\uparrow} + \hat{b}_{1,\downarrow})^\dagger(\hat{b}_{2,\uparrow} + \hat{b}_{2,\downarrow}) \\ & + (\hat{b}_{2,\uparrow} + \hat{b}_{2,\downarrow})^\dagger(\hat{b}_{1,\uparrow} + \hat{b}_{1,\downarrow})], \end{aligned} \quad (20)$$

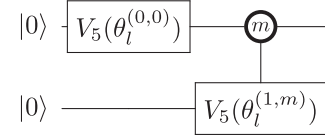


FIG. 4. A quantum circuit that prepares an arbitrary real wave function on two qu5its from an initial state $|0\rangle \otimes |0\rangle$. Four angles, $\theta_l^{(0,0)}$ are required to define the wave function on the first qu5it, and 20 angles, $\theta_l^{(1,m)}$, are required in the controlled rotation operator to define the four states of the second qu5it for each of the five states of the first qu5it (where $m = 0, 1, 2, 3, 4$ and $l = 0, 1, 2, 3$). The decomposition of the controlled-rotation operator is given in Fig. 5.

which, after reduction to Givens operators, becomes²

$$\begin{aligned} \hat{H}_2 = & [\varepsilon\hat{T}_z - (V+g)\hat{\mathcal{X}}_{13} - g\hat{N}_{\text{pairs}}] \otimes \hat{I}_5 \\ & + \hat{I}_5 \otimes [\varepsilon\hat{T}_z - (V+g)\hat{\mathcal{X}}_{13} - g\hat{N}_{\text{pairs}}] \\ & - V \sum_{r,s \in \{(12), (23)\}} (\hat{\mathcal{X}}_r \otimes \hat{\mathcal{X}}_s - \hat{\mathcal{Y}}_r \otimes \hat{\mathcal{Y}}_s) \\ & - \frac{g}{2} \sum_{r,s \in \{(01), (03), \\ & \quad -(14), -(34)\}} (\hat{\mathcal{X}}_r \otimes \hat{\mathcal{X}}_s + \hat{\mathcal{Y}}_r \otimes \hat{\mathcal{Y}}_s), \end{aligned} \quad (22)$$

where the negative signs in the second summation indices mean that the operator with the corresponding index has an additional minus sign. The energy densities of the two-qu5it systems, for the parameter sets defined in Eq. (9), are given in Table IV. While the ground state energy density is somewhat larger for $N = 4$ compared with $N = 2$, the energy densities of the excited states are substantially different.

The extreme case $V \gg g$ approaches the LMG model, in which the particles are distributed on mode pairs in states $\{|1\rangle, |2\rangle, |3\rangle\}$. In contrast, the case $V \ll g$ approaches the result of the two-level pairing model with particles being distributed among the states $\{|0\rangle, |1\rangle, |3\rangle, |4\rangle\}$ (states with paired spins).

1. State preparation on two qu5its

Preparing an arbitrary real wave function on the two-qu5it system is a straightforward extension of preparing such a state on two qubits, as can be found, e.g., in Ref. [121]. A quantum circuit for preparing a state on two qu5its is shown in Fig. 4, and is given in terms of single-qu5it rotations $\hat{V}_5(\theta_l^{(0,0)}) \otimes \hat{I}_5$ and controlled rotations $\hat{\Lambda}^{(m)} \otimes \hat{V}_5(\theta_l^{(1,m)})$, where $\hat{\Lambda}^{(m)}$ are projectors onto the m^{th} state in the qu5it Hilbert space. The form of the controlled rotation operator in terms of projectors on the first qu5it is given in Fig. 5. With 25 states in the Hilbert space, 24 angles are required to prepare a real wave function from some default state. With the quantum circuit shown in Fig. 4, we see that qu5it-0 (top qu5it in the figure) can be prepared with four angles (defining the corresponding five

²The notation of the summations is such that, for example,

$$\sum_{r,s \in \{(12), (23)\}} f_{r,s} = f_{12,12} + f_{12,23} + f_{23,12} + f_{23,23}. \quad (21)$$

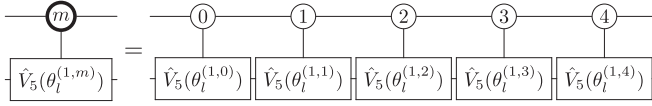


FIG. 5. The explicit construction of the controlled rotation operator shown in Fig. 4 in terms of projectors on the first qu5it.

amplitudes), while preparing qu5it-1 (bottom qu5it in Fig. 4) requires four angles per qu5it-0 state, hence a total of 20 angles, which provides the requisite 24 angles. Correspondingly, variational algorithms employed to establish the ground state (or excited states) of this system will, in the absence of further assumptions, require 24 angles.

The qu5it rotation operators \hat{V}_5 have the same form as Eq. (15). For example,

$$\hat{V}_5(\theta_i^{(1,3)}) = e^{-i\theta_3^{(1,3)}\hat{\chi}_{34}} e^{-i\theta_2^{(1,3)}\hat{\chi}_{23}} e^{-i\theta_1^{(1,3)}\hat{\chi}_{12}} e^{-i\theta_0^{(1,3)}\hat{\chi}_{01}}, \quad (23)$$

that enables the preparation of arbitrary real amplitudes on qu5it-1 from an initial state $|0\rangle$ (and with angles associated with a projection onto state $|3\rangle$ of qu5it-0).

2. Time evolution of two qu5its

The time evolution of the two-qu5it system is determined by the Hamiltonian in Eq. (22). As in the case of one qu5it, it contains noncommuting terms so that Trotterization will only approximate the time evolution. The resulting errors can, however, be systematically reduced by decreasing the time step Δt , or by using higher-order formulas. Considering the LO Trotterization of the evolution operator $\hat{U}(\Delta t)$, with one- and two-body contributions from the different interaction terms, gives

$$\hat{U}(\Delta t) = \hat{U}_2(\Delta t)\hat{U}_1(\Delta t), \quad (24)$$

where

$$\begin{aligned} \hat{U}_1(\Delta t) &= \hat{U}_1^{(\hat{T}_z)}(\Delta t)\hat{U}_1^{(\hat{\chi}_{13})}(\Delta t)\hat{U}_1^{(\hat{N}_{\text{pair}})}(\Delta t), \\ \hat{U}_1^{(\hat{T}_z)}(\Delta t) &= \prod_{j=1,2} e^{-i\Delta t\hat{T}_{z,j}}, \\ \hat{U}_1^{(\hat{\chi}_{13})}(\Delta t) &= \prod_{j=1,2} e^{+i\Delta t(V+g)\hat{\chi}_{13,j}}, \\ \hat{U}_1^{(\hat{N}_{\text{pair}})}(\Delta t) &= \prod_{j=1,2} e^{+i\Delta t g\hat{N}_{\text{pair},j}}, \end{aligned} \quad (25)$$

and

$$\begin{aligned} \hat{U}_2(\Delta t) &= \hat{U}_2^{(g)}(\Delta t)\hat{U}_2^{(V)}(\Delta t), \\ \hat{U}_2^{(V)}(\Delta t) &= \prod_{r,s \in \{(12), (23)\}} e^{+iV\Delta t\hat{\chi}_{r,1} \otimes \hat{\chi}_{s,2}} e^{-iV\Delta t\hat{Y}_{r,1} \otimes \hat{Y}_{s,2}}, \\ \hat{U}_2^{(g)}(\Delta t) &= \prod_{r,s \in \{(01), (03), \\ &\quad -(14), -(34)\}} e^{+i\frac{1}{2}g\Delta t\hat{\chi}_{r,1} \otimes \hat{\chi}_{s,2}} e^{+i\frac{1}{2}g\Delta t\hat{Y}_{r,1} \otimes \hat{Y}_{s,2}}. \end{aligned} \quad (26)$$

As these expressions are LO in the Trotter expansion, the presented order of operators in Eqs. (24), (25), and (26) has been chosen at random. In principle, all possible sequences of operator products could be explored in order to minimize Trotter errors in observables of interest for a given Trotter time step.

While the one-body terms can be implemented with phase operators and Givens rotations as discussed previously, the two-body entangling interactions are more complex. We discuss two possible implementations, based on gates that are available on current devices. One possibility is that qudit systems are able to perform two-qudit Givens rotation gates, as, for example, Mølmer-Sørensen gates in trapped-ion systems [86]. The other possibility is that generalized CNOT gates are available, such as in transmon-qudit systems [122,123]. This latter approach was studied in Ref. [100] for a qutrit-based system, and here we generalize it to higher-dimension qudits.

The quantum circuits require rotations on one of the qu5its controlled by the state of the other qu5it. These can be implemented via controlled \hat{X}_{ab} and \hat{Y}_{ab} gates, with

$$\hat{X}_{ab} = |a\rangle\langle b| + |b\rangle\langle a| + \sum_{c \neq \{a,b\}} |c\rangle\langle c|, \quad (27a)$$

$$\hat{Y}_{ab} = i(|a\rangle\langle b| - |b\rangle\langle a|) + \sum_{c \neq \{a,b\}} |c\rangle\langle c|. \quad (27b)$$

To be concrete, consider the action of an \hat{X}_{14} gate acting on qu5it-1 controlled by qu5it-0, which is implemented when qu5it-0 is in the state $|2\rangle$. This operation takes the form

$$[C\hat{X}]_{14}^2 = \hat{\Lambda}^{(2)} \otimes \hat{X}_{14} + \sum_{l \neq 2} \hat{\Lambda}^{(l)} \otimes \hat{I}_5. \quad (28)$$

The generalization to multiple control states is straightforward. For example, \hat{X}_{23} controlled by the states $|0\rangle, |1\rangle, |4\rangle$ reads

$$\begin{aligned} [C\hat{X}]_{23}^{0,1,4} &= \sum_{l \in \{0,1,4\}} \hat{\Lambda}^{(l)} \otimes \hat{X}_{23} + \sum_{l \neq \{0,1,4\}} \hat{\Lambda}^{(l)} \otimes \hat{I}_5 \\ &= [C\hat{X}]_{23}^0 [C\hat{X}]_{23}^1 [C\hat{X}]_{23}^4. \end{aligned} \quad (29)$$

The two types of required two-qu5it gates are $e^{-i\alpha\hat{\chi}_{ab} \otimes \hat{\chi}_{mn}}$ and $e^{-i\alpha\hat{Y}_{ab} \otimes \hat{Y}_{mn}}$, which can be implemented using the quantum circuits shown in Fig. 6. Additional simplifications, as shown in Fig. 7, can be made to reduce the number of controlled gates (this further reduces the number of controlled gates as the dimension of the qudit increases). After including these simplifications, and explicitly including the basis change, the circuits in Fig. 6 can be reduced to those in Fig. 8. While the circuits that are shown in Fig. 6 involve two G gates, eight $C\hat{X}$ or $C\hat{Y}$ gates, and four single qu5it gates, those in Fig. 8 contain two G gates and six $C\hat{X}$ or $C\hat{Y}$ gates. In the resource estimates that follow, we use the circuits in Fig. 8. These one- and two-body operators are sufficient to evolve a prepared state forward in time.

C. Arbitrary numbers of mode pairs

State preparation requires quantum circuits with a number of control operators that scales with the number of qu5its.

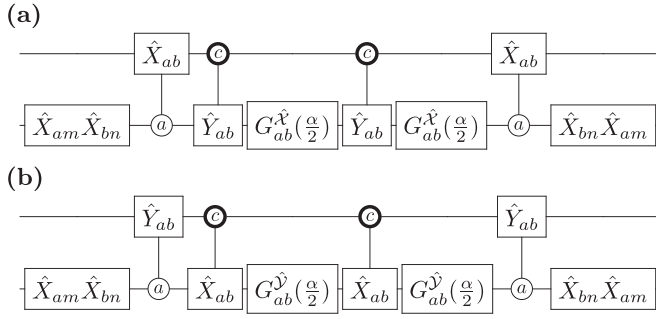


FIG. 6. Circuits for the two-qu5it entangling gates, with (a) implementing $G_{abmn}^{\hat{X}}(\alpha) = e^{-i\alpha\hat{X}_{ab}\otimes\hat{X}_{mn}}$, and (b) implementing $G_{abmn}^{\hat{Y}}(\alpha) = e^{-i\alpha\hat{Y}_{ab}\otimes\hat{Y}_{mn}}$. The index c on the controlled gates runs over the complement states of a and b (in a similar fashion to Fig. 5, but here $c \neq \{a, b\}$), and the Givens rotation $G_{ab}^{\hat{X}}(\frac{\alpha}{2})$ is defined as $e^{-i\frac{\alpha}{2}\hat{X}_{ab}}$ [similarly for $G_{ab}^{\hat{Y}}(\frac{\alpha}{2})$].

Without the concept of a distance between qu5its in this model, i.e., the all-to-all nature of the interactions, designs of localized circuits [124] with exponentially converging circuit truncations are not obvious. The high degree of symmetry in the Hamiltonian and the fact that the model is exactly solvable suggests, however, that simplifications in the state-preparation circuit and relations between the angles of the controlled operators seem likely. Reorganization of entanglement structures via application of, for example, the HL-VQE algorithm [38] could also potentially allow for efficient simulations of truncated systems, with exponential convergence towards the exact solution, as was obtained in the case of the LMG model. On the other hand, due to the quadratic form of the Agassi model Hamiltonian, only one- and two-body interactions are required in evolving the quantum state of an arbitrary number of modes forward in time. Thus, if the entangled states of interest can be reached from a tensor-product initial state, the one- and two-body circuits used to evolve two mode-pair systems forward, when implemented between all pairs of modes, are sufficient.

The required number of circuit elements per Trotter step can be determined for a system with $\Omega/2$ mode pairs. The number of one-body operators, assuming that the phase gates and Givens rotation can be implemented as fundamental gates, is $n_{1 \text{ mode pair}} = 3$. Counting gates in the quantum circuits shown in Fig. 8 (to implement the two-body operators) reveals that the total number of gates required is

$$n_{\frac{\Omega}{2} \text{ mode pairs}} = \frac{\Omega}{2} [1 G^{\hat{X}}, 2 \text{ Phase}] + \frac{1}{2} \frac{\Omega}{2} \left(\frac{\Omega}{2} - 1 \right) \times [120 C\hat{X}, 120 C\hat{Y}, 40 G^{\hat{X}}, 40 G^{\hat{Y}}], \quad (30)$$

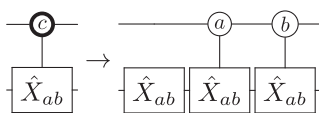


FIG. 7. Simplification for the multicoupled $C\hat{X}$ gates in Fig. 6, where the three controlled rotations (c runs over $c \neq \{a, b\}$) are replaced by two controlled rotations plus a single qu5it gate. The same simplification can be applied to the $C\hat{Y}$ gates.

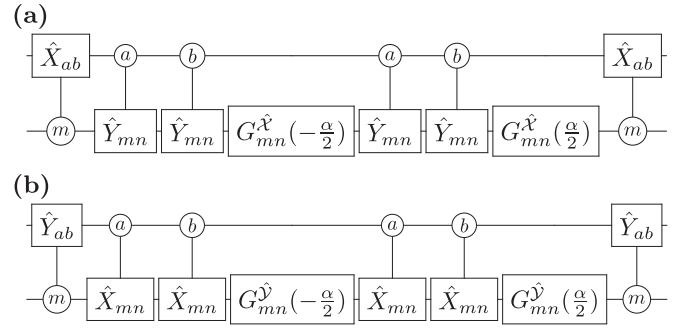


FIG. 8. Improved circuits for the two-qu5it entangling gates derived from those in Fig. 6, with (a) implementing $G_{abmn}^{\hat{X}}(\alpha) = e^{-i\alpha\hat{X}_{ab}\otimes\hat{X}_{mn}}$, and (b) implementing $G_{abmn}^{\hat{Y}}(\alpha) = e^{-i\alpha\hat{Y}_{ab}\otimes\hat{Y}_{mn}}$.

scaling, as expected, quadratically with the number of qu5its, and with sizable coefficients. This equation should be read as $20\Omega(\Omega - 2)$ controlled- \hat{X} gates, $10\Omega(\Omega - 2)$ single-qu5it Givens rotations, etc. The requirements are reduced significantly if two-qu5it Givens rotations are available, becoming

$$n_{\frac{\Omega}{2} \text{ mode pairs}} = \frac{\Omega}{2} [1 G^{\hat{X}}, 2 \text{ Phase}] + \frac{1}{2} \frac{\Omega}{2} \left(\frac{\Omega}{2} - 1 \right) \times [20 G^{\hat{X}\hat{X}}, 20 G^{\hat{Y}\hat{Y}}]. \quad (31)$$

For modest-size systems, the time dependence of an initial state can be determined exactly by matrix exponentiation. As an example, in Fig. 9, the exact time dependence of vacuum-to-vacuum survival amplitude, number of pairs, and $\langle \hat{S}_z \rangle$ from four sets of couplings, set-1 to set-4,³ are displayed in the $\Omega = 8$ system, for quenches from the two different tensor-product initial states given in Eq. (10): $|\psi(0)\rangle_A = |1\rangle^{\otimes 4}$ and $|\psi(0)\rangle_B = |4\rangle^{\otimes 2} \otimes |0\rangle^{\otimes 2}$. However, exact time evolution soon becomes unwieldy with increasing system size, and quantum simulations are required to extend to larger systems. A quantum simulation of this system can be accomplished with $\Omega/2 = 4$ qu5its (corresponding to a 625 dimensional Hilbert space) with quantum circuits implementing Trotter evolution, or variants thereof. If performed with previous JW qubit mappings [70,71], the analogous quantum simulation would require $4^{\Omega/2} = 16$ qubits (corresponding to a 65 536 dimensional Hilbert space).

It is informative to consider the exact time evolution over longer time intervals, beyond those shown in Fig. 9, as displayed in Appendix D. Observables evolving from $|\psi(0)\rangle_A$ are found to continue to rapidly oscillate at later times, while those from $|\psi(0)\rangle_B$ tend to fall more slowly toward their average long-time values, about which they slowly oscillate with amplitudes that decrease with increasing interaction strength. This behavior is consistent with $|\psi(0)\rangle_A$ being a spin-stretched ground state of the non-interacting Hamiltonian, with dominant overlap only onto a small number of states, as shown in Fig. 10(a). These are effectively *scar* states for this quenched system [125]. In contrast, the evolution from $|\psi(0)\rangle_B$, the initial state with energy that is in the middle of

³The set-0 is not displayed since it leads to a trivial time evolution.

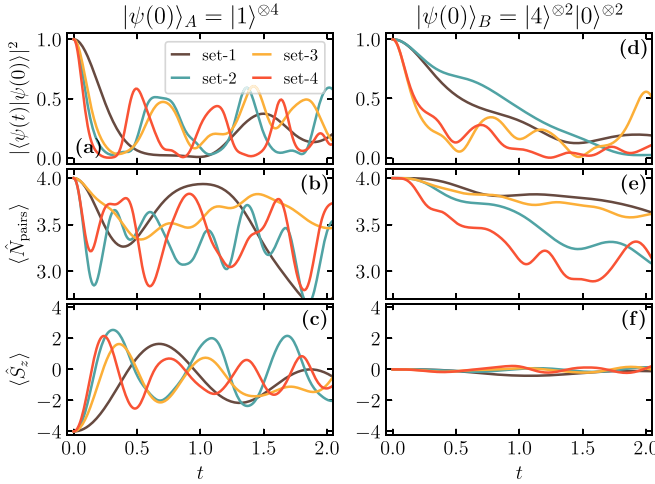


FIG. 9. The exact time dependence of (a), (d) $|\langle\psi(t)|\psi(0)\rangle|^2$, (b), (e) number of pairs, and (c), (f) $\langle\hat{S}_z\rangle$ for a system with $N = \Omega = 8$ particles for four sets of couplings, set-1 to set-4, given in Eq. (9). The left column is associated with the initial state $|\psi(0)\rangle_A$, while the right column is associated with $|\psi(0)\rangle_B$, as given in Eq. (10).

the excitation spectrum, is consistent with comparable overlap onto a large number of states, as shown in Fig. 10(b), giving multiple coherent contributions in time evolution. The exact wave functions for both initial configurations confirm these described structures. Interestingly, these different overlap structures suggest that they will incur different systematic errors in Trotterized time evolution when simulated with quantum computers and simulators. With multiple states contributing to time evolution, the errors from the system initially in $|\psi(0)\rangle_B$ are expected to be significantly larger than from starting in $|\psi(0)\rangle_A$, because of a “sign problem” in the form of incomplete cancellations between multiple amplitudes, as opposed to a few, in the unitary evolution. As we will show in subsequent sections, this is indeed the situation.

D. Quantum simulations using CIRQ-based classical simulation

With the developments presented in the previous sections, quantum simulations of these fundamentally five-dimensional systems can be implemented on quantum simulators of arrays

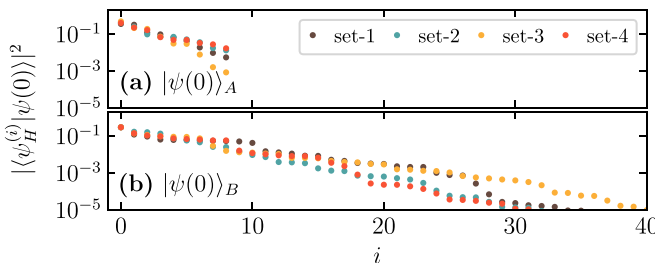


FIG. 10. Sorted nonzero overlaps between the initial state $|\psi(0)\rangle_{A/B}$ and the eigenstates of the Hamiltonian $|\psi_H^{(i)}\rangle$ for a system with $N = \Omega = 8$ particles and for the four sets of couplings. Top panel (a) shows $|\psi(0)\rangle_A$, and bottom panel (b) shows $|\psi(0)\rangle_B$.

of qu5its.⁴ Without access to a qu5it quantum computer at present, we used Google’s CIRQ software [126] to perform classical noiseless simulations for a selection of parameter sets and system sizes. The qudit capabilities of CIRQ form the foundation of a PYTHON-based [127] simulation code that furnishes single-thread⁵ single-CPU-node instances for qudit systems.

For the purposes of demonstration, we present results for the observables discussed above in a selection of system sizes for a range of LO Trotterizations of the evolution operators. In the simulations, we employed 1000 shots per run using the set-3 Hamiltonian couplings given in Eq. (9) and the two different initial states from Eq. (10), for systems of size $\{N_{q5} = 8, N = \Omega = 16\}$, $\{N_{q5} = 10, N = \Omega = 20\}$, corresponding to 16 and 20 particles distributed among eight and ten qu5its, respectively. These are compared with the time evolution of the full state-vector computed via exact exponentiation of the Hamiltonian, using the EXPKIT [129] package in JULIA [130].⁶ The results obtained for the $\Omega = 16$ system are shown in Figs. 11 and 12, and those for $\Omega = 20$ are shown in Figs. 13 and 14. We have also performed the simulation for the $\{N_{q5} = 12, \Omega = 24\}$ system, shown in Figs. 15 and 16. For this case, a comparison with the exact time evolution could not be accomplished using a single node, as it requires exponentiating $10^8 \times 10^8$ matrices. Simulations of larger systems ($\Omega > 24$) were not possible using the CIRQ-based PYTHON code on a single compute node of the University of Washington cluster Hyak (mox) due to memory limitations.

As expected, the Trotterized evolution curves for observables converge to the expected values as the number of Trotter steps becomes large over the explored time intervals. However, the convergence is faster for the initial state in which all the spin- \downarrow states are occupied, $|\psi(0)\rangle_A$. This can be understood to arise from Trotter errors being larger for the systems starting in $|\psi(0)\rangle_B$ than $|\psi(0)\rangle_A$ due to the larger number of comparable contributions to the unitary evolution (see Fig. 10), because of being higher in the energy spectrum, and the more substantial *sign problem* in forming their sum, as mentioned above. This is discussed in more detail in Appendix F. A potential way to improve the convergence of the Trotterization may be found by examining the breaking of symmetries. One of those is the exchange symmetry, since, for the original Hamiltonian \hat{H} , $[e^{-i\hat{H}}, \hat{P}_{ij}] = 0$, with \hat{P}_{ij} being the exchange operator of mode pairs i and j , but with the LO Trotterized operator $\hat{U}(t)$, as in Eq. (24), $[\hat{U}(t), \hat{P}_{ij}] \neq 0$. Similar issues have been found in other systems. For example, the Hamiltonian governing the evolution of dense coherent neutrino systems exhibits a similar exchange symmetry, and while Trotterization might break the symmetry, it can be

⁴In principle, they can also be straightforwardly implemented on devices with qudits with $d > 5$.

⁵The multithreaded high-performance version of CIRQ, QSIM [128], is still a qubit-based simulator, and does not support qudits (as of this writing).

⁶For the $\Omega = 20$ system, the Hamiltonian was projected to the $N = 20$ sector before exact exponentiation, reducing the dimension of the Hamiltonian matrix from 9 765 625 to 1 936 881.

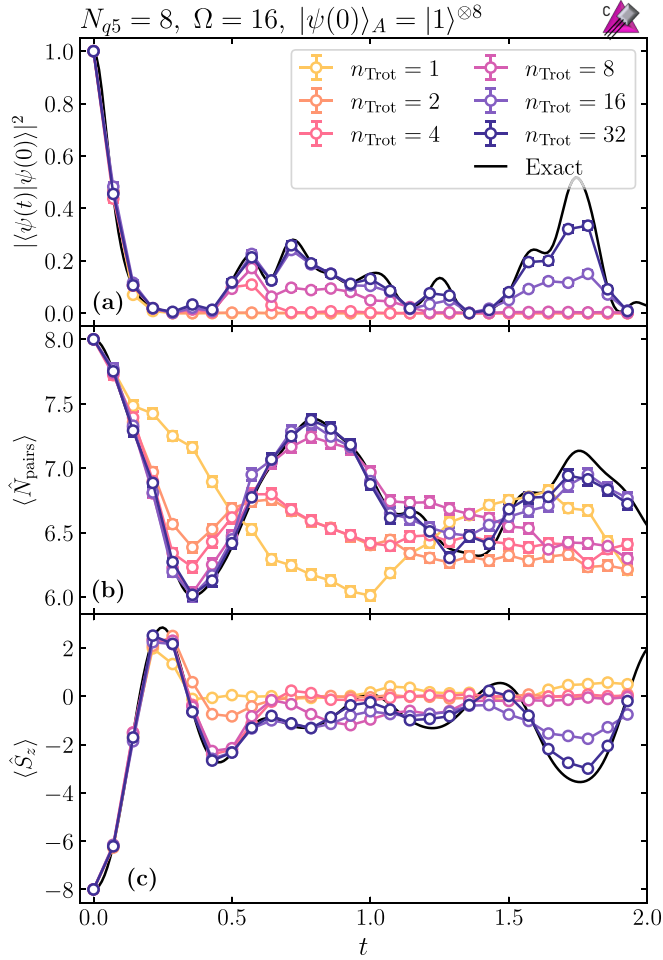


FIG. 11. The time dependence of (a) $|\langle\psi(t)|\psi(0)\rangle|^2$, (b) number of pairs, and (c) $\langle\hat{S}_z\rangle$, for set-3 of couplings [given in Eq. (9)] in a system with $N = 16$ particles initially in the state $|\psi(0)\rangle_A = |1\rangle^{\otimes 8}$. The different colors indicate different numbers of Trotter steps (n_{Trot}). The points are the results of noiseless classical simulation of the qu5it system with 10^3 shots. The icon denoting classical computation is defined in Ref. [121].

recovered [131]. A similar situation arises in simulations of 1 + 1-dimensional SU(3) lattice gauge theory [132] with n_f flavors of quarks, where Trotterization breaks global SU(3) symmetry.

Regarding the performance of the qudit simulator, Table I shows the time-to-solution (TtS) values for the different system sizes and number of Trotter steps considered in this work. The TtS is found to scale linearly with the number of Trotter steps, as expected, since the circuit depth increases linearly with n_{Trot} . For a fixed number of Trotter steps, when the system size is changed, we observe two different behaviors. For $\Omega \lesssim 16$, the TtS scales better than $5^{\Omega/2}$, while for $\Omega \gtrsim 16$ it scales approximately as $5^{\Omega/2}$. As the Hilbert space dimensionality of a 22-qu5it system is approximately that of a 50-qubit system, one anticipates that a quantum advantage may become accessible in systems with more than approximately 22 qu5its for certain observables. Gate-based classical simulations of systems

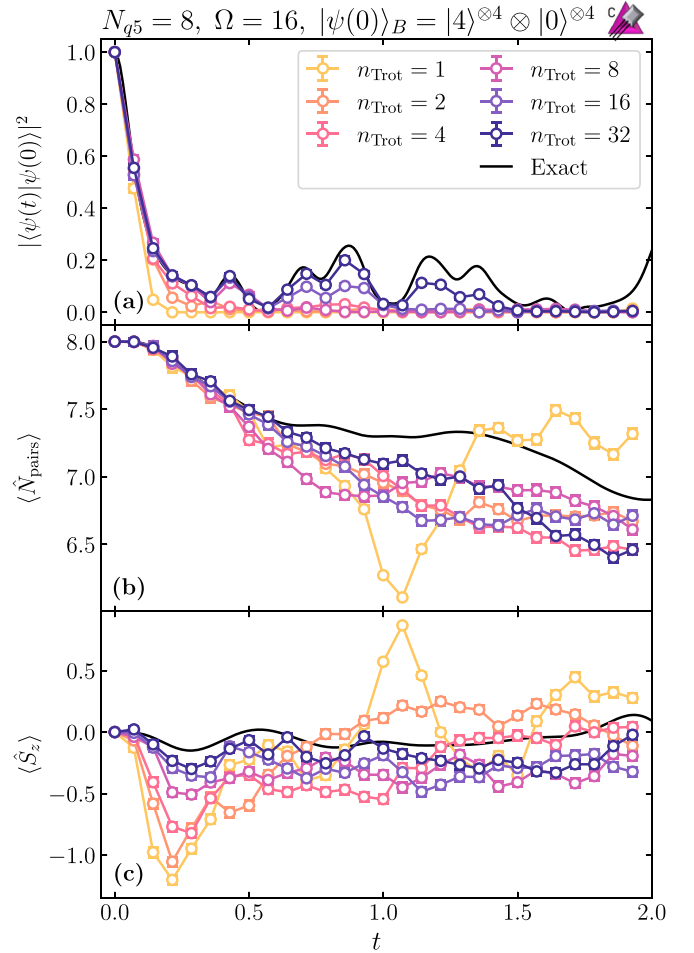


FIG. 12. The time dependence of (a) $|\langle\psi(t)|\psi(0)\rangle|^2$, (b) number of pairs, and (c) $\langle\hat{S}_z\rangle$, for set-3 of couplings [given in Eq. (9)] in a system with $N = 16$ particles initially in the state $|\psi(0)\rangle_B = |4\rangle^{\otimes 4} \otimes |0\rangle^{\otimes 4}$. The different colors indicate different numbers of Trotter steps (n_{Trot}). The points are the results of noiseless classical simulation of the qu5it system with 10^3 shots.

approaching this size are beyond the capability of a single-node simulation code, and will require large-scale parallel computation, as has already been accomplished in classical simulations of gate-based qubit systems [128,133–145]. The next step toward large-system simulations of qu5it

TABLE I. Time-to-solution (TtS) values (in seconds) for the qudit simulator for different system sizes (Ω) and Trotter steps (n_{Trot}). The code was executed on the University of Washington cluster Hyak (mox) on a single node and a single thread.

n_{Trot}	$\Omega = 8$	$\Omega = 12$	$\Omega = 16$	$\Omega = 20$	$\Omega = 24$
1	2	7	58	1921	66255
2	4	14	135	4803	166384
4	9	28	285	10448	364871
8	18	56	657	24005	759583
16	36	113	1347	43953	1539031
32	71	228	2683	89047	

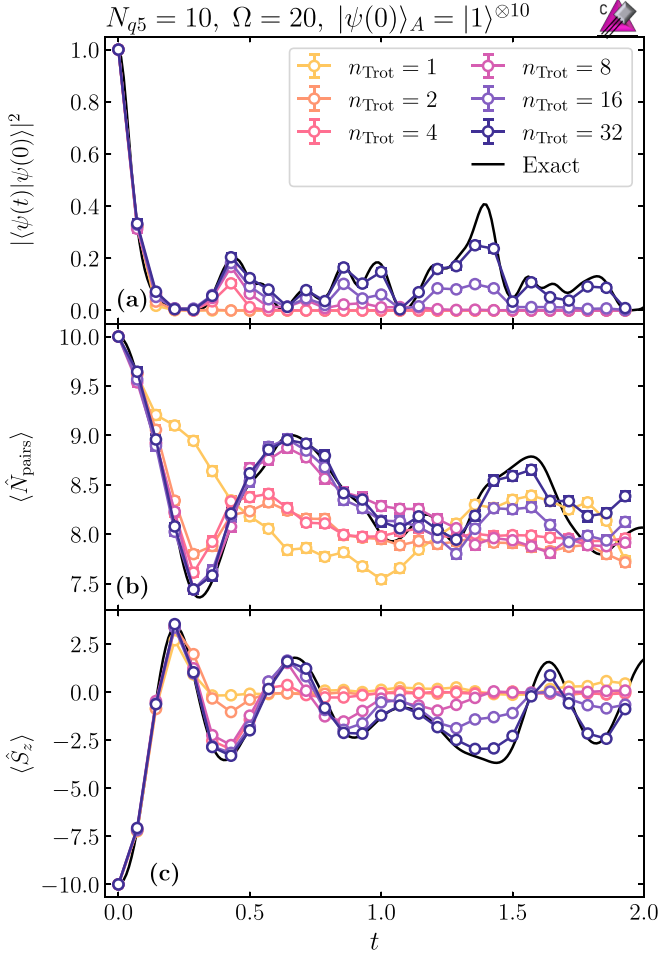


FIG. 13. The time dependence of (a) $|\langle\psi(t)|\psi(0)\rangle|^2$, (b) number of pairs, and (c) $\langle\hat{S}_z\rangle$, for set-3 of couplings [given in Eq. (9)] in a system with $N = 20$ particles initially in the state $|\psi(0)\rangle_A = |1\rangle^{\otimes 10}$. The different colors indicate different numbers of Trotter steps (n_{Trot}). The points are the results of noiseless classical simulation of the qu5it system with 10^3 shots.

systems is multinode parallelization that utilizes multiple GPUs per node.

IV. COMPARISON WITH QUBITS

As mentioned in the previous sections, the Agassi model was first mapped to qubits in Refs. [70,71]. In those works, a particular JW mapping assignment to qubits was considered. In order to compare the resource requirements for qubits with the requirements for qu5its, given in Sec. III C, two different mappings are considered here: (i) a physics-aware JW mapping (paJW) (that differs from that used in Refs. [70,71]) and (ii) a mapping using five levels of three qubits as a qu5it. In the paJW mapping, we have utilized the bosonic nature of mode pairs from the occupation involving only an even number of fermions to minimize JW strings of \hat{Z} operators between spins.

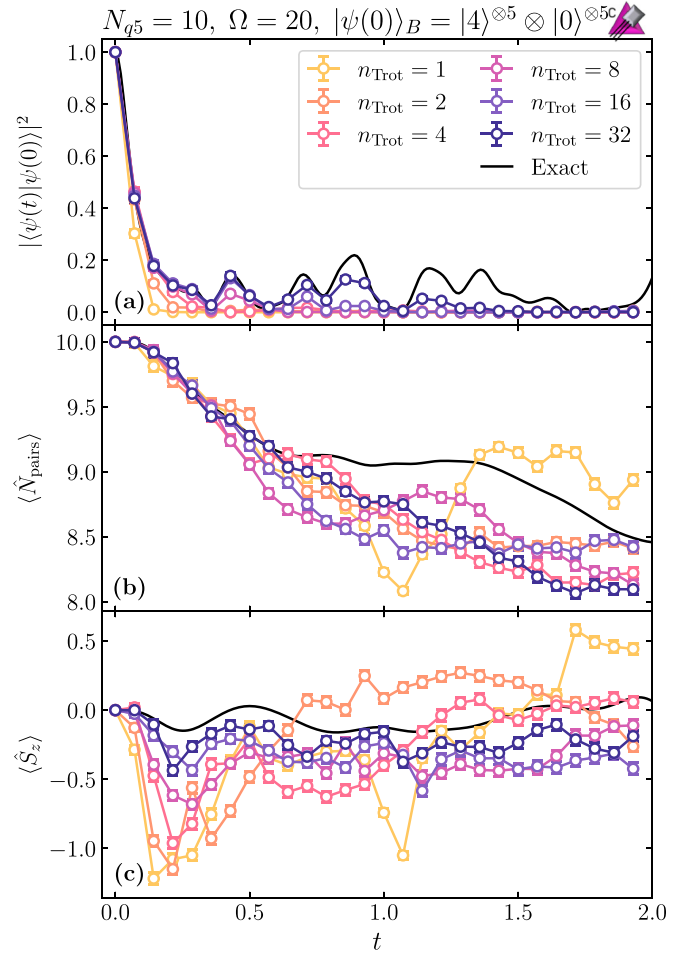


FIG. 14. The time dependence of (a) $|\langle\psi(t)|\psi(0)\rangle|^2$, (b) number of pairs, and (c) $\langle\hat{S}_z\rangle$, for set-3 of couplings [given in Eq. (9)] in a system with $N = 20$ particles initially in the state $|\psi(0)\rangle_B = |4\rangle^{\otimes 5} \otimes |0\rangle^{\otimes 5}$. The different colors indicate different numbers of Trotter steps (n_{Trot}). The points are the results of noiseless classical simulation of the qu5it system with 10^3 shots.

A. Physics-aware Jordan-Wigner mapping to qubits

A system of Ω modes can be simulated with 2Ω qubits using a JW mapping, in which an unoccupied state corresponds to a spin-down qubit, while an occupied state corresponds to a spin-up qubit. Such a mapping was used in the works of Refs. [70,71] to explore the one-mode-pair and two-mode-pair systems. We have found it convenient to implement a different ordering of states than used in those works, where we localize states in the same mode pair to be adjacent, in order to take better advantage of the approximate SO(5) symmetry. As the number of particles per mode pair is always even, there are no fermionic phases from operators moving across the lattice. The paJW mapping we have employed naturally encodes this feature, thereby minimizing the length of Pauli strings between operators.

For the one mode-pair system, requiring four qubits, the five states of the qu5it are mapped to the four qubits in the

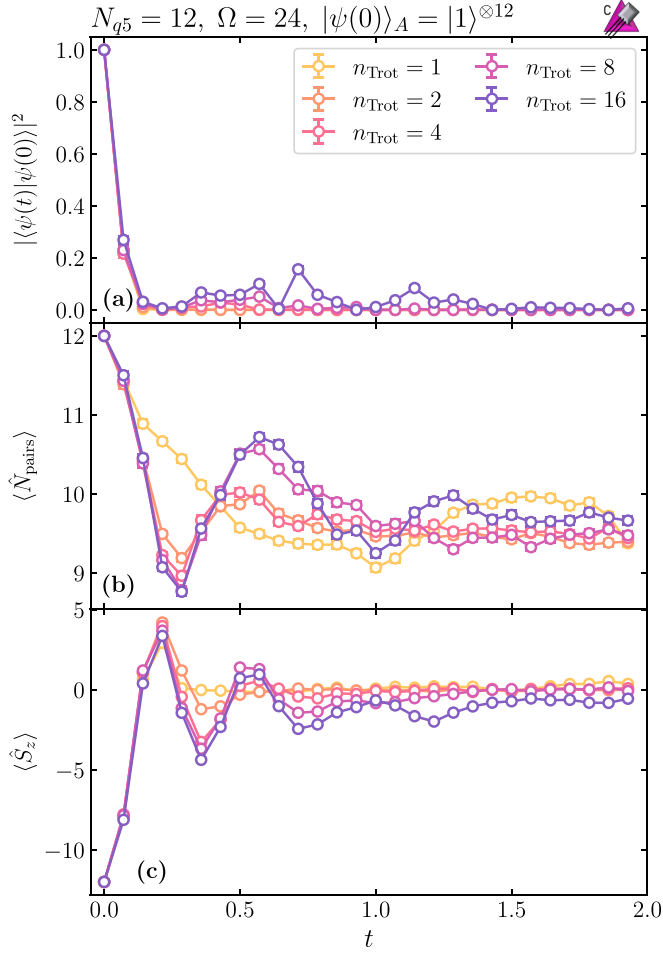


FIG. 15. The time dependence of (a) $|\langle\psi(t)|\psi(0)\rangle|^2$, (b) number of pairs, and (c) $\langle\hat{S}_z\rangle$, for set-3 of couplings [given in Eq. (9)] in a system with $N = 24$ particles initially in the state $|\psi(0)\rangle_A = |1\rangle^{\otimes 12}$. The different colors indicate different numbers of Trotter steps (n_{Trot}). The points are the results of noiseless classical simulation of the qu5it system with 10^3 shots.

paJW mapping as⁷

$$\begin{aligned} |0\rangle &\rightarrow |1111\rangle, & |1\rangle &\rightarrow |0101\rangle, \\ |2\rangle &\rightarrow \frac{1}{\sqrt{2}}[|0110\rangle + |1001\rangle], \\ |3\rangle &\rightarrow |1010\rangle, & |4\rangle &\rightarrow |0000\rangle. \end{aligned} \quad (32)$$

Figure 19 in Appendix E 1 a shows the quantum circuits for one step of LO Trotterized time evolution for one mode pair, which are well known from quantum chemistry and elsewhere [132,146]. The resource requirements of one Trotter step, in terms of number of Hadamard-gates, R_Z gates and CNOT gates, are

$$n_{1 \text{ mode pair}} = [2 H, 14 R_Z, 14 \text{ CNOT}]. \quad (33)$$

⁷In this mapping, an unoccupied state corresponds to spin-down which is identified as $|1\rangle$, while an occupied state is denoted by spin-up, denoted by $|0\rangle$.

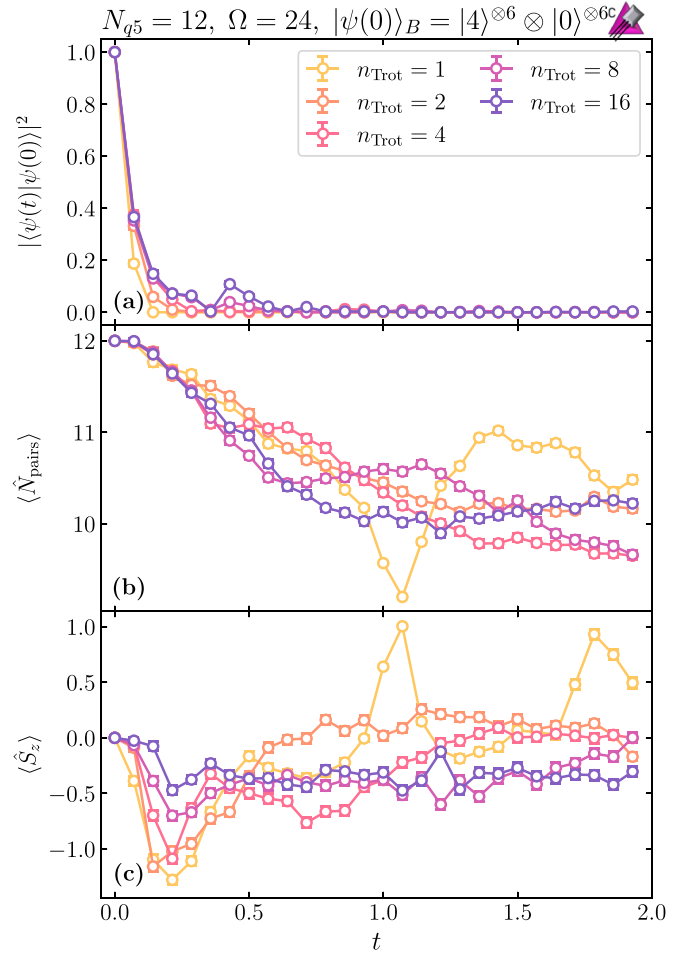


FIG. 16. The time dependence of (a) $|\langle\psi(t)|\psi(0)\rangle|^2$, (b) number of pairs, and (c) $\langle\hat{S}_z\rangle$, for set-3 of couplings [given in Eq. (9)] in a system with $N = 24$ particles initially in the state $|\psi(0)\rangle_B = |4\rangle^{\otimes 6} \otimes |0\rangle^{\otimes 6}$. The different colors indicate different numbers of Trotter steps (n_{Trot}). The points are the results of noiseless classical simulation of the qu5it system with 10^3 shots.

The time-evolution circuits for two mode pairs are given in Appendix E 1 b. The resources required to implement Trotterized time evolution from the terms in the Hamiltonian in Eq. (22) that act only on one mode pair are the same as given in the previous paragraph, and those required to implement the fundamentally two-mode-pair evolution are

$$n_{2 \text{ mode pairs}} = [16 H, 64 R_Z, 128 \text{ CNOT}]. \quad (34)$$

The resources for an arbitrary number, $\Omega/2$, of mode pairs follows straightforwardly,

$$\begin{aligned} n_{\frac{\Omega}{2} \text{ mode pairs}} &= \frac{\Omega}{2} [2 H, 14 R_Z, 14 \text{ CNOT}] \\ &+ \frac{1}{2} \frac{\Omega}{2} \left(\frac{\Omega}{2} - 1 \right) [16 H, 64 R_Z, 128 \text{ CNOT}], \end{aligned} \quad (35)$$

which will be distributed across a quantum register with 2Ω qubits (four qubits per mode pair).

B. State-to-state mapping to qubits

The Hilbert space of a qudit can be mapped to the space of multiple qubits, as is well known, in a state-to-state (StS) map. In our case, specifically for $d = 5$, the five states of a qu5it can be mapped onto five of the eight states of three qubits. We have chosen the binary mapping

$$\begin{aligned} |0\rangle &= |000\rangle, & |1\rangle &= |001\rangle, & |2\rangle &= |010\rangle, \\ |3\rangle &= |011\rangle, & |4\rangle &= |100\rangle, \end{aligned} \quad (36)$$

which best suits our physical system (other mappings are discussed in Appendix E 2).

The circuits required to perform time evolution of a single mode pair are given in Appendix E 2 a, with the following number of Hadamard gates, R_Z gates, and CNOT gates:

$$n_{1 \text{ mode pair}} = [2 H, 9 R_Z, 10 \text{ CNOT}]. \quad (37)$$

These gate requirements correspond to implementing one Givens rotation and two phase rotations for a single qu5it.

In the case of two mode pairs, the time-evolution circuits are given in Appendix E 2 b. The resource requirements in Table V show that this qubit mapping of two mode-pairs requires a substantial number of CNOT gates per Trotter step, in addition to comparable numbers of single qubit gates and rotations. From the discussions above, particularly the need for only two mode-pair interactions in a many-body system, the number of gates is found to be

$$n_{2 \text{ mode pairs}} = [32 H, 512 R_Z, 688 \text{ CNOT}], \quad (38)$$

which is approximately a factor of five greater in the number of entangling gates than the paJW mapping. The total resource requirements to simulate $\Omega/2$ pairs of modes with this mapping are

$$\begin{aligned} n_{\frac{\Omega}{2} \text{ mode pair}} &= \frac{\Omega}{2} [2 H, 9 R_Z, 10 \text{ CNOT}] \\ &+ \frac{1}{2} \frac{\Omega}{2} \left(\frac{\Omega}{2} - 1 \right) [32 H, 512 R_Z, 688 \text{ CNOT}]. \end{aligned} \quad (39)$$

C. Comparison between qu5it and qubit mappings

It is interesting to further compare the three mappings considered in this work, especially the size of the Hilbert space and number of entangling gates. Although we have not considered the effect of noisy hardware, these comparisons indicate how prone the different mappings are to errors.

Figure 17 shows the dimension of Hilbert space of different mappings as a function of the number of mode-pairs $\Omega/2$, as well as the total number of entangling gates, with CNOTs for qubits and $C\hat{X} + C\hat{Y}$ or $G^{\hat{x}\hat{x}} + G^{\hat{y}\hat{y}}$ for qu5its. The reduced dimensionality of the Hilbert space for qu5its compared to qubits, as clearly shown in Fig. 17(a), means that qu5its are much less susceptible than qubits to errors taking the system to unwanted regions of the Hilbert space. Importantly, all of the states in the qu5its are physically allowed states (state-changing errors, the equivalent of bit-flip errors, could move the state to a different particle number sector, which is still

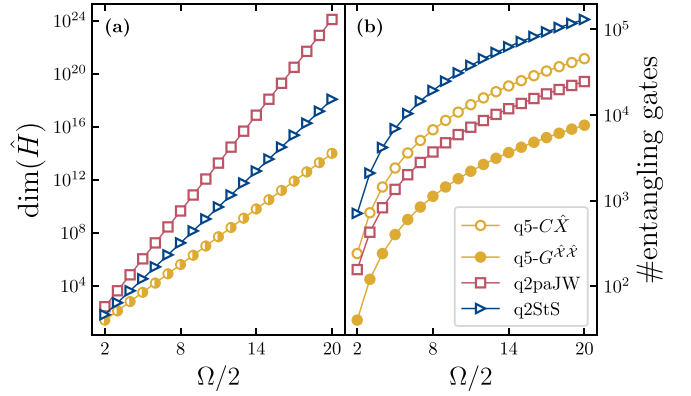


FIG. 17. A comparison of different mappings: qu5its (q5), qubits with paJW (q2paJW), and qubits with StS (q2StS). (a) Dimension of the Hilbert space as a function of the number of mode pairs. (b) Total number of entangling gates (for a single Trotter step) as a function of the number of mode pairs, with $C\hat{X}$ type or $G^{\hat{x}\hat{x}}$ type for qu5its, and CNOTs for qubits.

physically allowed, but prohibited due to the symmetries of the Hamiltonian), while the number of unphysical states in both qubit mappings grows exponentially with system size. Figure 17(b) displays the number of entangling gates required for the simulation of systems with increasing system size. If two-qu5it Givens rotations of the type $G^{\hat{x}\hat{x}}$ are directly implemented on the quantum device (plain yellow circles), the mapping to qu5its is the most advantageous in all aspects. Interestingly, if the two-qu5it Givens rotations are implemented via generalized $C\hat{X}$ -type gates, the paJW mapping requires fewer entangling gates than the mapping to qu5its. In that case, there would be a tradeoff to be made between the errors due to noise that take the system to unwanted parts of the Hilbert space, and those due to entangling gates of limited fidelity.

To quantify the impact of noise in the different simulation configurations, a realistic noisy simulator of qudit arrays [93,102], in addition to the existing ones for qubit systems, is required.

V. SUMMARY AND CONCLUSIONS

Pairing interactions between fermions in quantum many-body systems play a central role in important physical phenomena, ranging from structure of materials to the stability and decay of nuclei. Building upon our previous work, and pioneering studies by other authors, we have considered the quantum simulation of the Agassi model, which is a model of quantum systems with pairing and particle-hole interactions that extends the Lipkin-Meshkov-Glick model. The nature of the interactions is such that systems involving even numbers of particles are naturally embedded in an array of $d = 5$ qudits (qu5its) that make manifest the underlying SO(5) symmetry. The quantum circuits required to prepare entangled states and for time evolution of these systems are developed. They have been classically simulated using a code that we have developed on top of Google's CIRQ to examine the time dependence of spin, pairing, and persistence probabilities, starting

from two distinct initial tensor-product states: one that is the noninteracting ground state, and the other a highly excited configuration. The time evolutions of these states were found to exhibit quite different behaviors, originating from distinct decompositions onto eigenstates of the full Hamiltonian.

A comparison between resource requirements for simulations with qu5its and qubits is revealing. For the Agassi model, and for the mappings we have identified, there are advantages and disadvantages in choosing one over the other. The nature of the pairing is such that each mode pair can be mapped to a qu5it, and, with an even number of fermions occupying each qu5it at all times, the system can be considered to be a lattice simulation of a collection of bosons. While the qu5it array has a significantly smaller Hilbert space than for corresponding systems of qubits, depending on the available entangling gates, the number of such gates required for time evolution can be larger than for our paJW mapping onto four qubits per mode pair, but less than for a StS mapping onto three qubits per mode pair.

A simulation of the Agassi model with 20 mode pairs (for a single Trotter step) requires either 10 qu5its and 45.6k (where k denotes $\times 10^3$) entangling gates (or 7.6k two-qu5it Givens rotations), or 80 qubits and 24.6k entangling gates (paJW), or 60 qubits and 130.9k entangling gates (StS). These resource requirements indicate that there is no “clear winner” between qu5its and qubits for simulating the Agassi model. If both types of quantum computers were available, the choice of which to utilize depends on the overall performance of the hardware, which could be assessed with a series of tests and benchmarks [147]. There have been impressive recent advances in developing qudit systems across a number of platforms, e.g., trapped-ion, NV centers, superconducting, and SRF-cavity systems. It will be interesting to assess the performance of emerging qudit systems in simulations of the types of systems considered in this work. The advantages gained through a greatly reduced Hilbert space in qu5it systems will be partially offset by the increased number of entangling gates required for time evolution. Benchmarking such devices with the Agassi model will establish another codesign vector for improving available qudit hardware (which is anticipated to mostly consist of improving the qudit entangling gates), to evolve and eventually outperform available qubit systems.

There is a clear need for improving classical simulation capabilities of qudit systems, including in the number of qudits that can be addressed, in the speed at which Trotter evolution can be executed, and in the quality of the noise models. With groups developing classical simulation codes for qubit systems, the analogous capabilities for qudit arrays is lagging, largely because the quantum devices are not readily accessible, but this is expected to change in the future. We intend to extend the performance of our code to heterogeneous-node parallelization.

There is a more general lesson that can be learned from our analysis of the time evolution starting from a low-lying state compared to a high-lying one. The Trotter errors associated with the high-lying state are larger because of the larger number of states making comparable contributions to the evolution. In particular, at any given time, there are contributions from multiple amplitudes, with cancellations that are

disturbed by the Trotter errors. The more amplitudes there are with cancellations, the more significant are such errors. More generally, such sign problems will also manifest themselves as signal-to-noise problems due to device noise. These sign problems will be important in studies of, for example, high-energy fragmentation [148–151] in QCD, for which there are many energetically accessible states, or coupled channels, that will contribute with comparable amplitudes to the time evolution.

Finally, while the present work has focused on the use of symmetry considerations to guide mappings to qudits, we have not attempted to investigate and optimize the entanglement structures of the systems under study. While a quantitative understanding of entanglement between systems of qubits is now well advanced and studies of entanglement between systems of qutrits continues to develop, our work motivates further studies related to the entanglement of qudit systems. Early pioneering work on entanglement in fermionic paired systems [10] has shown that pairing is not equivalent to entanglement of the whole state, nor its two-particle reduced density matrix, but manifests as a different type of quantum correlation. The model we have studied here and mapped to systems of qu5its provides an explicit quantum system to further study such quantum correlations. An optimization of the entanglement structure between mode pairs could potentially be achieved by developing entanglement-driven algorithms, such as the HL-VQE algorithm [38] which we plan to extend to qudit systems in the near future. Such entanglement rearrangement, combined with the symmetry-informed mappings developed in this work, could further improve the efficiency of the quantum simulations.

The results shown in figures can be found in a Github repository [152].

ACKNOWLEDGMENTS

We would like to thank Anthony Ciavarella, Roland Farrell, and Momme Hengstenberg for helpful discussions, and for all of our other colleagues and collaborators that provide the platform from which this work has emerged. Martin Savage would like to thank the High-Energy Physics group at Universität Bielefeld for kind hospitality during some of this work. The authors also acknowledge support by the Deutsche Forschungsgemeinschaft (DFG, German Research Foundation) through the CRC-TR 211 “Strong-interaction matter under extreme conditions,” Project No. 315477589–TRR 211. This work was supported, in part, by Universität Bielefeld and the ERC-885281-KILONOVA Advanced Grant (C.E.P.R.), by the U.S. Department of Energy, Office of Science, Office of Nuclear Physics, Inqubator for Quantum Simulation (IQuS) under Awards No. DOE (NP) and No. DE-SC0020970 (M.J.S.), and the Quantum Science Center (QSC) [153], a National Quantum Information Science Research Center of the U.S. Department of Energy (M.I.). This work was enabled, in part, by the use of advanced computational, storage, and networking infrastructure provided by the Hyak supercomputer system at the University of Washington [154], and was also supported, in part, through the Department of Physics [155] and the College of Arts and Sciences [156] at the University of Washington. We are very appreciative of comments

made by an anonymous referee, regarding a simplification of controlled-qu5it gates. The circuit compression resulting from

this observation is shown in Figs. 7 and 8, and led to a modest reduction in quantum resources required for time evolution.

APPENDIX A: MATRIX REPRESENTATION OF THE SO(5) GENERATORS

The basis states defined in Eq. (7),

$$\left\{ |0000\rangle, |1010\rangle, \frac{1}{\sqrt{2}}(|0110\rangle + |1001\rangle), |0101\rangle, |1111\rangle \right\} = \{ |0\rangle, |1\rangle, |2\rangle, |3\rangle, |4\rangle \}, \quad (\text{A1})$$

are given in terms of the occupation of the two states per mode encapsulated in one qu5it, $|n_{k\downarrow}, n_{k\uparrow}, n_{-k\downarrow}, n_{-k\uparrow}\rangle$. When written in terms of the action of fermionic creation operators, they have the form

$$\begin{aligned} |0\rangle &= |\phi\rangle, & |1\rangle &= c_{k,\downarrow}^\dagger c_{-k,\downarrow}^\dagger |\phi\rangle, & |2\rangle &= \frac{1}{\sqrt{2}}(c_{k,\uparrow}^\dagger c_{-k,\downarrow}^\dagger + c_{k,\downarrow}^\dagger c_{-k,\uparrow}^\dagger) |\phi\rangle, \\ |3\rangle &= c_{k,\uparrow}^\dagger c_{-k,\uparrow}^\dagger |\phi\rangle, & |4\rangle &= c_{k,\downarrow}^\dagger c_{k,\uparrow}^\dagger c_{-k,\downarrow}^\dagger c_{-k,\uparrow}^\dagger |\phi\rangle, \end{aligned} \quad (\text{A2})$$

where $|\phi\rangle$ denotes the vacuum state of the qu5it (all states are unoccupied). In this basis, the matrix representations of the operators defined in Eq. (6) are (omitting the k label)

$$\begin{aligned} T_+ &= \sqrt{2} \begin{pmatrix} 0 & 0 & 0 & 0 & 0 \\ 0 & 0 & 0 & 0 & 0 \\ 0 & 1 & 0 & 0 & 0 \\ 0 & 0 & 1 & 0 & 0 \\ 0 & 0 & 0 & 0 & 0 \end{pmatrix}, & T_- &= \sqrt{2} \begin{pmatrix} 0 & 0 & 0 & 0 & 0 \\ 0 & 0 & 1 & 0 & 0 \\ 0 & 0 & 0 & 1 & 0 \\ 0 & 0 & 0 & 0 & 0 \\ 0 & 0 & 0 & 0 & 0 \end{pmatrix}, & T_z &= \begin{pmatrix} 0 & 0 & 0 & 0 & 0 \\ 0 & -1 & 0 & 0 & 0 \\ 0 & 0 & 0 & 0 & 0 \\ 0 & 0 & 0 & 1 & 0 \\ 0 & 0 & 0 & 0 & 0 \end{pmatrix}, \\ b_\uparrow &= \begin{pmatrix} 0 & 0 & 0 & 1 & 0 \\ 0 & 0 & 0 & 0 & -1 \\ 0 & 0 & 0 & 0 & 0 \\ 0 & 0 & 0 & 0 & 0 \\ 0 & 0 & 0 & 0 & 0 \end{pmatrix}, & b_\downarrow &= \begin{pmatrix} 0 & 1 & 0 & 0 & 0 \\ 0 & 0 & 0 & 0 & 0 \\ 0 & 0 & 0 & 0 & 0 \\ 0 & 0 & 0 & 0 & -1 \\ 0 & 0 & 0 & 0 & 0 \end{pmatrix}, & b_z &= \begin{pmatrix} 0 & 0 & 1 & 0 & 0 \\ 0 & 0 & 0 & 0 & 0 \\ 0 & 0 & 0 & 0 & 1 \\ 0 & 0 & 0 & 0 & 0 \\ 0 & 0 & 0 & 0 & 0 \end{pmatrix}, \\ b_\uparrow^\dagger &= \begin{pmatrix} 0 & 0 & 0 & 0 & 0 \\ 0 & 0 & 0 & 0 & 0 \\ 0 & 0 & 0 & 0 & 0 \\ 1 & 0 & 0 & 0 & 0 \\ 0 & -1 & 0 & 0 & 0 \end{pmatrix}, & b_\downarrow^\dagger &= \begin{pmatrix} 0 & 0 & 0 & 0 & 0 \\ 1 & 0 & 0 & 0 & 0 \\ 0 & 0 & 0 & 0 & 0 \\ 0 & 0 & 0 & 0 & 0 \\ 0 & 0 & 0 & -1 & 0 \end{pmatrix}, & b_z^\dagger &= \begin{pmatrix} 0 & 0 & 0 & 0 & 0 \\ 0 & 0 & 0 & 0 & 0 \\ 1 & 0 & 0 & 0 & 0 \\ 0 & 0 & 0 & 0 & 0 \\ 0 & 0 & 1 & 0 & 0 \end{pmatrix}, \\ N &= \begin{pmatrix} 0 & 0 & 0 & 0 & 0 \\ 0 & 2 & 0 & 0 & 0 \\ 0 & 0 & 2 & 0 & 0 \\ 0 & 0 & 0 & 2 & 0 \\ 0 & 0 & 0 & 0 & 4 \end{pmatrix}, \end{aligned} \quad (\text{A3})$$

which constitute a set of ten generators of SO(5). The commutation relations between these operators are given in Table II.

Some of the entries in Table II make use of the operators given in Eq. (A4),

$$\begin{aligned} \hat{N}_\uparrow &= \frac{\hat{N}}{2} + \hat{T}_z, & \hat{N}_\downarrow &= \frac{\hat{N}}{2} - \hat{T}_z, \\ \tilde{N}_\uparrow &= \hat{N}_\uparrow - \frac{\hat{\Omega}_5}{2}, & \tilde{N}_\downarrow &= \hat{N}_\downarrow - \frac{\hat{\Omega}_5}{2}, & \tilde{N} &= \frac{1}{2}(\tilde{N}_\uparrow + \tilde{N}_\downarrow) = \frac{1}{2}(\hat{N} - \hat{\Omega}_5), \\ \hat{\Omega}_5 &= \frac{1}{5} \text{Tr}(\hat{N}) \hat{I}_5. \end{aligned} \quad (\text{A4})$$

TABLE II. The commutation relations between the ten SO(5) generators with matrix representations given in Eq. (A3). The commutator at the intersection of row (a) and column (b) is ordered as [row (a), column (b)].

	T_+	T_-	T_z	b_\uparrow	b_\downarrow	b_z	b_\uparrow^\dagger	b_\downarrow^\dagger	b_z^\dagger	N
T_+	0	$2T_z$	$-T_+$	$-\sqrt{2}b_z$	0	$-\sqrt{2}b_\downarrow$	0	$\sqrt{2}b_z^\dagger$	$\sqrt{2}b_\uparrow^\dagger$	0
T_-		0	T_-	0	$-\sqrt{2}b_z$	$-\sqrt{2}b_\uparrow$	$\sqrt{2}b_z^\dagger$	0	$\sqrt{2}b_\downarrow^\dagger$	0
T_z			0	$-b_\uparrow$	b_\downarrow	0	b_\uparrow^\dagger	$-b_\downarrow^\dagger$	0	0
b_\uparrow				0	0	0	$-\tilde{N}_\uparrow$	0	$-T_-/\sqrt{2}$	$2b_\uparrow$
b_\downarrow					0	0	0	$-\tilde{N}_\downarrow$	$-T_+/\sqrt{2}$	$2b_\downarrow$
b_z						0	$-T_+/\sqrt{2}$	$-T_-/\sqrt{2}$	$-\tilde{N}$	$2b_z$
b_\uparrow^\dagger							0	0	0	$-2b_\uparrow^\dagger$
b_\downarrow^\dagger								0	0	$-2b_\downarrow^\dagger$
b_z^\dagger									0	$-2b_z^\dagger$
N										0

Generators in their standard form, normalized to $\text{Tr}(T_a T_b) = 2\delta_{ab}$, are defined through linear combinations of the generators in Eq. (A3),

$$\begin{aligned}
 T_1 &= \frac{1}{2}(T_+ + T_-) = \frac{1}{\sqrt{2}} \begin{pmatrix} 0 & 0 & 0 & 0 & 0 \\ 0 & 0 & 1 & 0 & 0 \\ 0 & 1 & 0 & 1 & 0 \\ 0 & 0 & 1 & 0 & 0 \\ 0 & 0 & 0 & 0 & 0 \end{pmatrix}, & T_2 &= \frac{1}{2i}(T_+ - T_-) = \frac{i}{\sqrt{2}} \begin{pmatrix} 0 & 0 & 0 & 0 & 0 \\ 0 & 0 & 1 & 0 & 0 \\ 0 & -1 & 0 & 1 & 0 \\ 0 & 0 & -1 & 0 & 0 \\ 0 & 0 & 0 & 0 & 0 \end{pmatrix}, \\
 T_3 &= T_z = \begin{pmatrix} 0 & 0 & 0 & 0 & 0 \\ 0 & -1 & 0 & 0 & 0 \\ 0 & 0 & 0 & 0 & 0 \\ 0 & 0 & 0 & 1 & 0 \\ 0 & 0 & 0 & 0 & 0 \end{pmatrix}, & T_4 &= \frac{1}{\sqrt{2}}(b_\downarrow^\dagger + b_\downarrow) = \frac{1}{\sqrt{2}} \begin{pmatrix} 0 & 1 & 0 & 0 & 0 \\ 1 & 0 & 0 & 0 & 0 \\ 0 & 0 & 0 & 0 & 0 \\ 0 & 0 & 0 & 0 & -1 \\ 0 & 0 & 0 & -1 & 0 \end{pmatrix}, \\
 T_5 &= \frac{1}{i\sqrt{2}}(b_\downarrow^\dagger - b_\downarrow) = \frac{i}{\sqrt{2}} \begin{pmatrix} 0 & 1 & 0 & 0 & 0 \\ -1 & 0 & 0 & 0 & 0 \\ 0 & 0 & 0 & 0 & 0 \\ 0 & 0 & 0 & 0 & -1 \\ 0 & 0 & 0 & 1 & 0 \end{pmatrix}, & T_6 &= \frac{1}{\sqrt{2}}(b_\uparrow^\dagger + b_\uparrow) = \frac{1}{\sqrt{2}} \begin{pmatrix} 0 & 0 & 0 & 1 & 0 \\ 0 & 0 & 0 & 0 & -1 \\ 0 & 0 & 0 & 0 & 0 \\ 1 & 0 & 0 & 0 & 0 \\ 0 & -1 & 0 & 0 & 0 \end{pmatrix}, \\
 T_7 &= \frac{1}{i\sqrt{2}}(b_\uparrow^\dagger - b_\uparrow) = \frac{i}{\sqrt{2}} \begin{pmatrix} 0 & 0 & 0 & 1 & 0 \\ 0 & 0 & 0 & 0 & -1 \\ 0 & 0 & 0 & 0 & 0 \\ -1 & 0 & 0 & 0 & 0 \\ 0 & 1 & 0 & 0 & 0 \end{pmatrix}, & T_8 &= \frac{1}{\sqrt{2}}(b_z^\dagger + b_z) = \frac{1}{\sqrt{2}} \begin{pmatrix} 0 & 0 & 1 & 0 & 0 \\ 0 & 0 & 0 & 0 & 0 \\ 1 & 0 & 0 & 0 & 1 \\ 0 & 0 & 0 & 0 & 0 \\ 0 & 0 & 1 & 0 & 0 \end{pmatrix}, \\
 T_9 &= \frac{1}{i\sqrt{2}}(b_z^\dagger - b_z) = \frac{i}{\sqrt{2}} \begin{pmatrix} 0 & 0 & 1 & 0 & 0 \\ 0 & 0 & 0 & 0 & 0 \\ -1 & 0 & 0 & 0 & 1 \\ 0 & 0 & 0 & 0 & 0 \\ 0 & 0 & -1 & 0 & 0 \end{pmatrix}, & T_{10} &= \frac{1}{2}[N - \Omega_5] = \begin{pmatrix} -1 & 0 & 0 & 0 & 0 \\ 0 & 0 & 0 & 0 & 0 \\ 0 & 0 & 0 & 0 & 0 \\ 0 & 0 & 0 & 0 & 0 \\ 0 & 0 & 0 & 0 & 1 \end{pmatrix}, \tag{A5}
 \end{aligned}$$

with their commutators given in Table III.

TABLE III. The commutation relations between the ten SO(5) generators with matrix representations given in Eq. (A5). The commutator at the intersection of row (a) and column (b) is ordered as [row (a), column (b)].

	T_1	T_2	T_3	T_4	T_5	T_6	T_7	T_8	T_9	T_{10}
T_1	0	iT_3	$-iT_2$	$iT_9/\sqrt{2}$	$-iT_8/\sqrt{2}$	$iT_9/\sqrt{2}$	$-iT_8/\sqrt{2}$	$i(T_7 + T_5)/\sqrt{2}$	$-i(T_6 + T_4)/\sqrt{2}$	0
T_2		0	iT_1	$-iT_8/\sqrt{2}$	$-iT_9/\sqrt{2}$	$iT_8/\sqrt{2}$	$iT_9/\sqrt{2}$	$i(T_4 - T_6)/\sqrt{2}$	$i(T_5 - T_7)/\sqrt{2}$	0
T_3			0	$-iT_5$	iT_4	iT_7	$-iT_6$	0	0	0
T_4				0	$i\tilde{N}_\downarrow$	0	0	$-iT_2/\sqrt{2}$	$iT_1/\sqrt{2}$	$-iT_5$
T_5					0	0	0	$-iT_1/\sqrt{2}$	$-iT_2/\sqrt{2}$	iT_4
T_6						0	$i\tilde{N}_\uparrow$	$iT_2/\sqrt{2}$	$iT_1/\sqrt{2}$	$-iT_7$
T_7							0	$-iT_1/\sqrt{2}$	$iT_2/\sqrt{2}$	iT_6
T_8								0	iT_{10}	$-iT_9$
T_9									0	iT_8
T_{10}										0

Further, a set of L_{ij} 's can be defined as linear combinations of the T_i 's,

$$\begin{aligned}
 T_1 = L_{12}, \quad T_2 = L_{23}, \quad T_3 = L_{31}, \quad T_4 = -\frac{1}{\sqrt{2}}(L_{15} + L_{34}), \quad T_5 = \frac{1}{\sqrt{2}}(L_{14} - L_{35}), \\
 T_6 = \frac{1}{\sqrt{2}}(L_{34} - L_{15}), \quad T_7 = \frac{1}{\sqrt{2}}(L_{14} + L_{35}), \quad T_8 = L_{24}, \quad T_9 = L_{25}, \quad T_{10} = L_{54},
 \end{aligned} \tag{A6}$$

such that (with $L_{ij} = -L_{ji}$)

$$[L_{ij}, L_{kl}] = i(\delta_{jk}L_{il} + \delta_{il}L_{jk} - \delta_{jl}L_{ik} - \delta_{ik}L_{jl}). \tag{A7}$$

APPENDIX B: SPECTRUM OF THE AGASSI MODEL

The energies of the lowest-lying states in the Agassi model for the sets of couplings in Eq. (9) and for a selection of mode-pair number and occupancy are given in Table IV.

APPENDIX C: MATRIX REPRESENTATION OF SINGLE-QU5IT GIVENS OPERATORS

The matrix representations of selected \mathcal{X}_{ij} Givens operators for a single qu5it are

$$\begin{aligned}
 \mathcal{X}_{01} = \begin{pmatrix} 0 & 1 & 0 & 0 & 0 \\ 1 & 0 & 0 & 0 & 0 \\ 0 & 0 & 0 & 0 & 0 \\ 0 & 0 & 0 & 0 & 0 \\ 0 & 0 & 0 & 0 & 0 \end{pmatrix}, \quad \mathcal{X}_{03} = \begin{pmatrix} 0 & 0 & 0 & 1 & 0 \\ 0 & 0 & 0 & 0 & 0 \\ 0 & 0 & 0 & 0 & 0 \\ 1 & 0 & 0 & 0 & 0 \\ 0 & 0 & 0 & 0 & 0 \end{pmatrix}, \quad \mathcal{X}_{12} = \begin{pmatrix} 0 & 0 & 0 & 0 & 0 \\ 0 & 0 & 1 & 0 & 0 \\ 0 & 1 & 0 & 0 & 0 \\ 0 & 0 & 0 & 0 & 0 \\ 0 & 0 & 0 & 0 & 0 \end{pmatrix}, \\
 \mathcal{X}_{14} = \begin{pmatrix} 0 & 0 & 0 & 0 & 0 \\ 0 & 0 & 0 & 0 & 1 \\ 0 & 0 & 0 & 0 & 0 \\ 0 & 0 & 0 & 0 & 0 \\ 0 & 1 & 0 & 0 & 0 \end{pmatrix}, \quad \mathcal{X}_{23} = \begin{pmatrix} 0 & 0 & 0 & 0 & 0 \\ 0 & 0 & 0 & 0 & 0 \\ 0 & 0 & 0 & 1 & 0 \\ 0 & 0 & 1 & 0 & 0 \\ 0 & 0 & 0 & 0 & 0 \end{pmatrix}, \quad \mathcal{X}_{34} = \begin{pmatrix} 0 & 0 & 0 & 0 & 0 \\ 0 & 0 & 0 & 0 & 0 \\ 0 & 0 & 0 & 0 & 0 \\ 0 & 0 & 0 & 0 & 1 \\ 0 & 0 & 0 & 1 & 0 \end{pmatrix},
 \end{aligned} \tag{C1}$$

and selected \mathcal{Y}_{ij} Givens operators are

$$\begin{aligned}
 \mathcal{Y}_{01} = i \begin{pmatrix} 0 & -1 & 0 & 0 & 0 \\ 1 & 0 & 0 & 0 & 0 \\ 0 & 0 & 0 & 0 & 0 \\ 0 & 0 & 0 & 0 & 0 \\ 0 & 0 & 0 & 0 & 0 \end{pmatrix}, \quad \mathcal{Y}_{03} = i \begin{pmatrix} 0 & 0 & 0 & -1 & 0 \\ 0 & 0 & 0 & 0 & 0 \\ 0 & 0 & 0 & 0 & 0 \\ 1 & 0 & 0 & 0 & 0 \\ 0 & 0 & 0 & 0 & 0 \end{pmatrix}, \quad \mathcal{Y}_{12} = i \begin{pmatrix} 0 & 0 & 0 & 0 & 0 \\ 0 & 0 & -1 & 0 & 0 \\ 0 & 1 & 0 & 0 & 0 \\ 0 & 0 & 0 & 0 & 0 \\ 0 & 0 & 0 & 0 & 0 \end{pmatrix}, \\
 \mathcal{Y}_{14} = i \begin{pmatrix} 0 & 0 & 0 & 0 & 0 \\ 0 & 0 & 0 & 0 & -1 \\ 0 & 0 & 0 & 0 & 0 \\ 0 & 0 & 0 & 0 & 0 \\ 0 & 1 & 0 & 0 & 0 \end{pmatrix}, \quad \mathcal{Y}_{23} = i \begin{pmatrix} 0 & 0 & 0 & 0 & 0 \\ 0 & 0 & 0 & 0 & 0 \\ 0 & 0 & 0 & -1 & 0 \\ 0 & 0 & 1 & 0 & 0 \\ 0 & 0 & 0 & 0 & 0 \end{pmatrix}, \quad \mathcal{Y}_{34} = i \begin{pmatrix} 0 & 0 & 0 & 0 & 0 \\ 0 & 0 & 0 & 0 & 0 \\ 0 & 0 & 0 & 0 & 0 \\ 0 & 0 & 0 & 0 & -1 \\ 0 & 0 & 0 & 1 & 0 \end{pmatrix}.
 \end{aligned} \tag{C2}$$

TABLE IV. The energy density, $\mathcal{E}_i = E_i/\Omega$ (average energy per mode), of the ground state and the first- and second-excited states of the Agassi model for the sets of parameters defined in the text, (ε, V, g) : set-0 = (1.0, 0.0, 0.0), set-1 = (1.0, 0.5, 0.5), set-2 = (1.0, 1.5, 0.5), set-3 = (1.0, 0.5, 1.5), set-4 = (1.0, 1.5, 1.5).

Ω	N	Quantity	set-0	set-1	set-2	set-3	set-4
2	0	\mathcal{E}_0	0.000	0.000	0.000	0.000	0.000
2	2	\mathcal{E}_0	-0.500	-0.957	-1.368	-1.868	-2.331
2	2	\mathcal{E}_1	0.000	0.000	0.000	0.000	0.000
2	2	\mathcal{E}_2	0.500	0.457	0.868	0.368	0.831
2	4	\mathcal{E}_0	0.000	-0.500	-0.500	-1.500	-1.500
4	0	\mathcal{E}_0	0.000	0.000	0.000	0.000	0.000
4	2	\mathcal{E}_0	-0.250	-0.701	-0.923	-1.660	-1.902
4	2	\mathcal{E}_1	-0.250	-0.280	-0.451	-0.280	-0.451
4	2	\mathcal{E}_2	0.000	0.000	0.000	0.000	0.000
4	4	\mathcal{E}_0	-0.500	-1.125	-1.797	-2.495	-3.007
4	4	\mathcal{E}_1	-0.250	-0.684	-1.400	-1.166	-1.896
4	4	\mathcal{E}_2	-0.250	-0.376	-0.480	-0.858	-0.855
4	6	\mathcal{E}_0	-0.250	-0.951	-1.173	-2.410	-2.652
4	6	\mathcal{E}_1	-0.250	-0.530	-0.701	-1.030	-1.201
4	6	\mathcal{E}_2	0.000	-0.250	-0.250	-0.750	-0.750
4	8	\mathcal{E}_0	0.000	-0.500	-0.500	-1.500	-1.500
6	0	\mathcal{E}_0	0.000	0.000	0.000	0.000	0.000
6	2	\mathcal{E}_0	-0.167	-0.623	-0.777	-1.600	-1.764
6	2	\mathcal{E}_1	-0.167	-0.186	-0.300	-0.186	-0.300
6	2	\mathcal{E}_2	-0.167	-0.186	-0.300	-0.186	-0.300
6	4	\mathcal{E}_0	-0.333	-1.068	-1.492	-2.672	-3.012
6	4	\mathcal{E}_1	-0.333	-0.615	-1.098	-1.268	-1.761
6	4	\mathcal{E}_2	-0.333	-0.607	-1.060	-1.183	-1.500
6	6	\mathcal{E}_0	-0.500	-1.325	-2.363	-3.201	-3.723
6	6	\mathcal{E}_1	-0.333	-1.052	-2.257	-1.934	-2.991
6	6	\mathcal{E}_2	-0.333	-0.766	-1.100	-1.607	-2.049
6	8	\mathcal{E}_0	-0.333	-1.234	-1.659	-3.171	-3.512
6	8	\mathcal{E}_1	-0.333	-0.782	-1.265	-1.768	-2.261
6	8	\mathcal{E}_2	-0.333	-0.773	-1.227	-1.683	-2.000
6	10	\mathcal{E}_0	-0.167	-0.956	-1.110	-2.600	-2.764
6	10	\mathcal{E}_1	-0.167	-0.520	-0.634	-1.186	-1.300
6	10	\mathcal{E}_2	-0.167	-0.520	-0.634	-1.186	-1.300
6	12	\mathcal{E}_0	0.000	-0.500	-0.500	-1.500	-1.500
8	0	\mathcal{E}_0	0.000	0.000	0.000	0.000	0.000
8	2	\mathcal{E}_0	-0.125	-0.587	-0.705	-1.572	-1.696
8	2	\mathcal{E}_1	-0.125	-0.140	-0.225	-0.140	-0.225
8	2	\mathcal{E}_2	-0.125	-0.140	-0.225	-0.140	-0.225
8	4	\mathcal{E}_0	-0.250	-1.042	-1.350	-2.755	-3.010
8	4	\mathcal{E}_1	-0.250	-0.583	-0.948	-1.323	-1.694
8	4	\mathcal{E}_2	-0.250	-0.580	-0.901	-1.285	-1.515
8	6	\mathcal{E}_0	-0.375	-1.365	-2.057	-3.543	-3.936
8	6	\mathcal{E}_1	-0.375	-1.034	-1.919	-2.222	-3.000
8	6	\mathcal{E}_2	-0.375	-0.878	-1.688	-2.028	-2.400
8	8	\mathcal{E}_0	-0.500	-1.547	-3.041	-3.933	-4.456
8	8	\mathcal{E}_1	-0.375	-1.349	-3.017	-2.669	-3.900
8	8	\mathcal{E}_2	-0.375	-1.104	-1.735	-2.379	-3.168
8	10	\mathcal{E}_0	-0.375	-1.490	-2.182	-3.918	-4.311
8	10	\mathcal{E}_1	-0.375	-1.159	-2.044	-2.597	-3.375
8	10	\mathcal{E}_2	-0.375	-1.003	-1.813	-2.403	-2.775
8	12	\mathcal{E}_0	-0.250	-1.292	-1.600	-3.505	-3.760

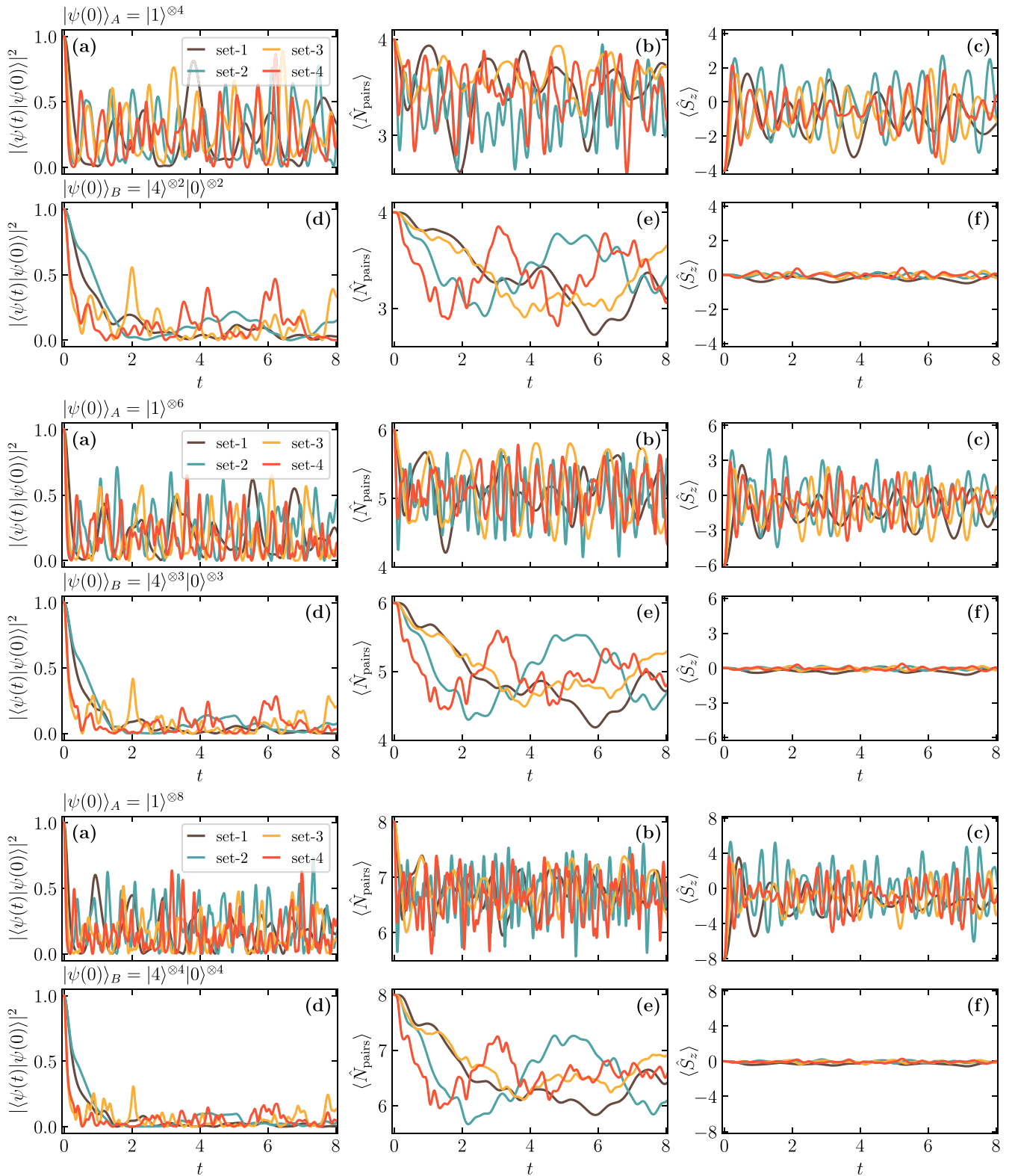
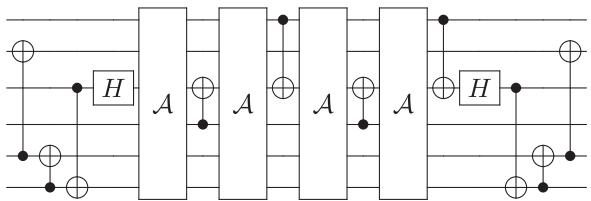
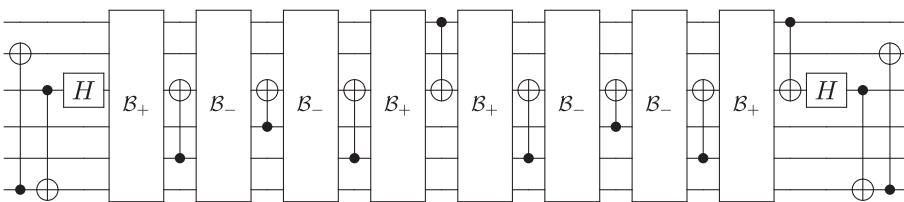


FIG. 18. The exact time dependence of (a), (d) $|\langle \psi(t) | \psi(0) \rangle|^2$, (b), (e) number of pairs, and (c), (f) $\langle \hat{S}_z \rangle$ for a system with $N = \Omega = 8$ particles (rows 1–2), $N = \Omega = 12$ particles (rows 3–4), and $N = \Omega = 16$ particles (rows 5–6), for four sets of couplings, set-1 to set-4, given in Eq. (9). For the different panels, (a)–(c) are associated with the initial state $|\psi(0)\rangle_A$, while (d)–(f) are associated with $|\psi(0)\rangle_B$, as given in Eq. (10).

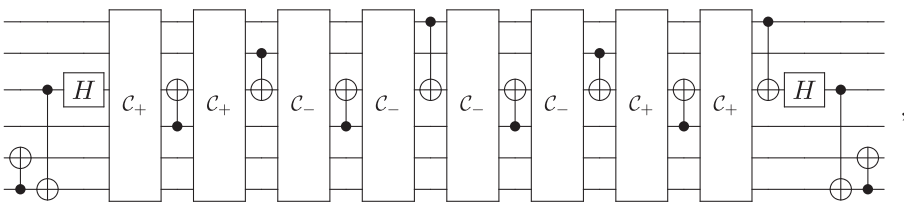
The circuits that implement the time evolution induced by each term are the following:

(a) :  ,

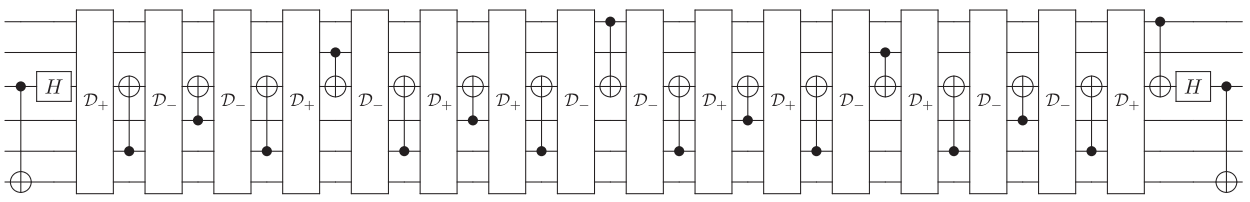
$$A = \begin{array}{c} \text{---} \\ \text{---} \\ \text{---} \\ \text{---} \end{array} \begin{array}{c} \boxed{R_Z(\delta)} \oplus \\ \boxed{R_Z(-\delta)} \oplus \\ \boxed{R_Z(-\delta)} \oplus \\ \boxed{R_Z(\delta)} \oplus \end{array} \begin{array}{c} \text{---} \\ \text{---} \\ \text{---} \\ \text{---} \end{array} \begin{array}{c} \boxed{R_Z(\delta)} \oplus \\ \boxed{R_Z(-\delta)} \oplus \\ \boxed{R_Z(-\delta)} \oplus \\ \boxed{R_Z(\delta)} \oplus \end{array} \begin{array}{c} \text{---} \\ \text{---} \\ \text{---} \\ \text{---} \end{array} \begin{array}{c} \boxed{R_Z(\delta)} \oplus \\ \boxed{R_Z(-\delta)} \oplus \\ \boxed{R_Z(-\delta)} \oplus \\ \boxed{R_Z(\delta)} \oplus \end{array} \begin{array}{c} \text{---} \\ \text{---} \\ \text{---} \\ \text{---} \end{array} \quad , \quad (\text{E19a})$$

(b) :  ,

$$B_{\pm} = \begin{array}{c} \text{---} \\ \text{---} \\ \text{---} \\ \text{---} \end{array} \begin{array}{c} \boxed{R_Z(\pm\delta)} \oplus \\ \boxed{R_Z(\mp\delta)} \oplus \\ \boxed{R_Z(\mp\delta)} \oplus \\ \boxed{R_Z(\pm\delta)} \oplus \end{array} \begin{array}{c} \text{---} \\ \text{---} \\ \text{---} \\ \text{---} \end{array} \begin{array}{c} \boxed{R_Z(\pm\delta)} \oplus \\ \boxed{R_Z(\mp\delta)} \oplus \\ \boxed{R_Z(\mp\delta)} \oplus \\ \boxed{R_Z(\pm\delta)} \oplus \end{array} \begin{array}{c} \text{---} \\ \text{---} \\ \text{---} \\ \text{---} \end{array} \begin{array}{c} \boxed{R_Z(\pm\delta)} \oplus \\ \boxed{R_Z(\mp\delta)} \oplus \\ \boxed{R_Z(\mp\delta)} \oplus \\ \boxed{R_Z(\pm\delta)} \oplus \end{array} \begin{array}{c} \text{---} \\ \text{---} \\ \text{---} \\ \text{---} \end{array} \quad , \quad (\text{E19b})$$

(c) :  ,

$$c_{\pm} = \begin{array}{c} \text{---} \\ \text{---} \\ \text{---} \\ \text{---} \end{array} \begin{array}{c} \boxed{R_Z(\pm\delta)} \oplus \\ \boxed{R_Z(\mp\delta)} \oplus \\ \boxed{R_Z(\pm\delta)} \oplus \\ \boxed{R_Z(\mp\delta)} \oplus \end{array} \begin{array}{c} \text{---} \\ \text{---} \\ \text{---} \\ \text{---} \end{array} \begin{array}{c} \boxed{R_Z(\pm\delta)} \oplus \\ \boxed{R_Z(\mp\delta)} \oplus \\ \boxed{R_Z(\pm\delta)} \oplus \\ \boxed{R_Z(\mp\delta)} \oplus \end{array} \begin{array}{c} \text{---} \\ \text{---} \\ \text{---} \\ \text{---} \end{array} \begin{array}{c} \boxed{R_Z(\pm\delta)} \oplus \\ \boxed{R_Z(\mp\delta)} \oplus \\ \boxed{R_Z(\pm\delta)} \oplus \\ \boxed{R_Z(\mp\delta)} \oplus \end{array} \begin{array}{c} \text{---} \\ \text{---} \\ \text{---} \\ \text{---} \end{array} \quad , \quad (\text{E19c})$$

(d) :  ,

$$D_{\pm} = \begin{array}{c} \text{---} \\ \text{---} \\ \text{---} \\ \text{---} \end{array} \begin{array}{c} \boxed{R_Z(\pm\delta)} \oplus \\ \boxed{R_Z(\pm\delta)} \oplus \end{array} \begin{array}{c} \text{---} \\ \text{---} \\ \text{---} \\ \text{---} \end{array} \begin{array}{c} \boxed{R_Z(\pm\delta)} \oplus \\ \boxed{R_Z(\pm\delta)} \oplus \end{array} \begin{array}{c} \text{---} \\ \text{---} \\ \text{---} \\ \text{---} \end{array} \quad , \quad (\text{E19d})$$

with $\delta = -tV/8$. The resources required to execute these circuits are shown in Table V, where the g terms are also included, as they have a similar structure. There are two exceptions, since there are terms with five and six $\hat{\sigma}^{\pm}$. For example,

TABLE V. Resource requirements to perform one Trotter step of time evolution for each two-mode-pair term in the Hamiltonian given in Eq. (E16). The “(*)” items from the g terms have the same structure as those from the $2V$ terms, and therefore can be grouped together.

	H	R_Z	CNOT
$\hat{\Lambda}_0^{(0)}\hat{\sigma}_1^+\hat{\sigma}_2^-\hat{\Lambda}_3^{(0)}\hat{\sigma}_4^+\hat{\sigma}_5^- + \text{H.c.}$	2	32	42
$\hat{\Lambda}_0^{(0)}\hat{\sigma}_1^+\hat{\sigma}_2^-\hat{\Lambda}_3^{(0)}\hat{\Lambda}_4^{(1)}\hat{\sigma}_5^+ + \text{H.c.}$	2	32	44
$\hat{\Lambda}_0^{(0)}\hat{\Lambda}_1^{(1)}\hat{\sigma}_2^+\hat{\Lambda}_3^{(0)}\hat{\sigma}_4^+\hat{\sigma}_5^- + \text{H.c.}$	2	32	44
$\hat{\Lambda}_0^{(0)}\hat{\Lambda}_1^{(1)}\hat{\sigma}_2^+\hat{\Lambda}_3^{(0)}\hat{\Lambda}_4^{(1)}\hat{\sigma}_5^+ + \text{H.c.}$	2	32	50
(*) $\hat{\Lambda}_0^{(0)}\hat{\sigma}_1^-\hat{\sigma}_2^-\hat{\Lambda}_3^{(0)}\hat{\sigma}_4^+\hat{\sigma}_5^+ + \text{H.c.}$	2	32	42
(*) $\hat{\Lambda}_0^{(0)}\hat{\sigma}_1^-\hat{\sigma}_2^-\hat{\Lambda}_3^{(0)}\hat{\Lambda}_4^{(0)}\hat{\sigma}_5^+ + \text{H.c.}$	2	32	44
$\hat{\Lambda}_0^{(0)}\hat{\sigma}_1^-\hat{\sigma}_2^-\hat{\sigma}_3^+\hat{\Lambda}_4^{(0)}\hat{\sigma}_5^- + \text{H.c.}$	2	32	42
$\hat{\Lambda}_0^{(0)}\hat{\sigma}_1^-\hat{\sigma}_2^-\hat{\sigma}_3^+\hat{\sigma}_4^-\hat{\sigma}_5^- + \text{H.c.}$	2	32	42
(*) $\hat{\Lambda}_0^{(0)}\hat{\Lambda}_1^{(0)}\hat{\sigma}_2^-\hat{\Lambda}_3^{(0)}\hat{\sigma}_4^+\hat{\sigma}_5^+ + \text{H.c.}$	2	32	44
(*) $\hat{\Lambda}_0^{(0)}\hat{\Lambda}_1^{(0)}\hat{\sigma}_2^-\hat{\Lambda}_3^{(0)}\hat{\Lambda}_4^{(0)}\hat{\sigma}_5^+ + \text{H.c.}$	2	32	50
$\hat{\Lambda}_0^{(0)}\hat{\Lambda}_1^{(0)}\hat{\sigma}_2^-\hat{\sigma}_3^+\hat{\Lambda}_4^{(0)}\hat{\sigma}_5^- + \text{H.c.}$	2	32	44
$\hat{\Lambda}_0^{(0)}\hat{\Lambda}_1^{(0)}\hat{\sigma}_2^-\hat{\sigma}_3^+\hat{\sigma}_4^-\hat{\sigma}_5^- + \text{H.c.}$	2	32	42
$\hat{\sigma}_0^-\hat{\Lambda}_1^{(0)}\hat{\sigma}_2^+\hat{\Lambda}_3^{(0)}\hat{\sigma}_4^+\hat{\sigma}_5^+ + \text{H.c.}$	2	32	42
$\hat{\sigma}_0^-\hat{\Lambda}_1^{(0)}\hat{\sigma}_2^+\hat{\Lambda}_3^{(0)}\hat{\Lambda}_4^{(0)}\hat{\sigma}_5^+ + \text{H.c.}$	2	32	44
$\hat{\sigma}_0^-\hat{\Lambda}_1^{(0)}\hat{\sigma}_2^+\hat{\sigma}_3^+\hat{\Lambda}_4^{(0)}\hat{\sigma}_5^- + \text{H.c.}$	2	32	42
$\hat{\sigma}_0^-\hat{\Lambda}_1^{(0)}\hat{\sigma}_2^+\hat{\sigma}_3^+\hat{\sigma}_4^-\hat{\sigma}_5^- + \text{H.c.}$	2	32	42
$\hat{\sigma}_0^-\hat{\sigma}_1^+\hat{\sigma}_2^+\hat{\Lambda}_3^{(0)}\hat{\sigma}_4^+\hat{\sigma}_5^+ + \text{H.c.}$	2	32	42
$\hat{\sigma}_0^-\hat{\sigma}_1^+\hat{\sigma}_2^+\hat{\Lambda}_3^{(0)}\hat{\Lambda}_4^{(0)}\hat{\sigma}_5^+ + \text{H.c.}$	2	32	42
$\hat{\sigma}_0^-\hat{\sigma}_1^+\hat{\sigma}_2^+\hat{\sigma}_3^+\hat{\Lambda}_4^{(0)}\hat{\sigma}_5^- + \text{H.c.}$	2	32	42
$\hat{\sigma}_0^-\hat{\sigma}_1^+\hat{\sigma}_2^+\hat{\sigma}_3^+\hat{\sigma}_4^-\hat{\sigma}_5^- + \text{H.c.}$	2	32	42
Total	32	512	688

$$e^{itg(\hat{\Lambda}_0^{(0)}\hat{\sigma}_1^-\hat{\sigma}_2^-\hat{\sigma}_3^+\hat{\sigma}_4^-\hat{\sigma}_5^- + \text{H.c.})} = \text{Circuit Diagram} , \quad (\text{E20a})$$

The circuit diagram for the Trotter step consists of two main parts. The top part shows a sequence of operations on five qubits. It starts with a Hadamard gate on the top qubit, followed by a series of CNOT gates and entangling gates \mathcal{E}_+ and \mathcal{E}_- . The bottom part defines the entangling gates \mathcal{E}_\pm as a sequence of eight R_Z gates with alternating phases $\pm\zeta$ and $\mp\zeta$, connected by CNOT gates.

$$e^{itg(\hat{\sigma}_0^- \hat{\sigma}_1^+ \hat{\sigma}_2^+ \hat{\sigma}_3^+ \hat{\sigma}_4^- \hat{\sigma}_5^- + \text{H.c.})} = \begin{array}{c} \text{---} \\ \text{---} \\ \text{---} \\ \text{---} \\ \text{---} \\ \text{---} \\ \text{---} \end{array} \begin{array}{c} H \\ \oplus \\ \oplus \\ \oplus \\ \oplus \\ \oplus \\ \oplus \end{array} \begin{array}{c} \mathcal{F}_+ \\ \mathcal{F}_+ \\ \mathcal{F}_- \\ \mathcal{F}_- \end{array} \begin{array}{c} \oplus \\ \oplus \\ \oplus \\ \oplus \\ \oplus \\ \oplus \\ \oplus \end{array} \begin{array}{c} H \\ \oplus \\ \oplus \\ \oplus \\ \oplus \\ \oplus \\ \oplus \end{array} \text{---} , \\ \\ \mathcal{F}_\pm = \begin{array}{c} \text{---} \\ \text{---} \\ \text{---} \\ \text{---} \\ \text{---} \\ \text{---} \\ \text{---} \end{array} \begin{array}{c} R_Z(\pm\zeta) \\ R_Z(\pm\zeta) \\ R_Z(\mp\zeta) \\ R_Z(\mp\zeta) \\ R_Z(\mp\zeta) \\ R_Z(\mp\zeta) \\ R_Z(\pm\zeta) \\ R_Z(\pm\zeta) \end{array} \text{---} , \quad (\text{E20b})$$

with $\zeta = -tg/16$. Note that these decompositions are not unique, as different definitions of the G operators are possible, and other forms may be more efficient depending on the connectivity of the quantum computer.

APPENDIX F: A SIGN PROBLEM IN QUANTUM SIMULATIONS: TROTTERIZED TIME EVOLUTION AND DEVICE NOISE

By considering Trotterized time evolution, we have identified a potential sign problem in quantum simulations of observables determined from many contributing states. Disturbances to cancellations between contributing amplitudes result from a combination of device errors, which can be Pauli twirled towards incoherence (contributing statistical noise) [157], and systematic algorithmic errors, such as from Trotterization. In the case of statistical noise, this sign problem will manifest as a signal-to-noise (StN) problem. Sign and StN problems plague classical lattice gauge theory calculations of systems at finite density or with finite baryon number [158–168]. The hope continues to be that some or all of these types of problems will be absent or mitigated in quantum simulations that will allow for progress to be made that is not possible for classical lattice QCD, including ground- and excited-state preparation, as well as time evolution, of nuclei (even modestly sized nuclei). A similar hope is present for simulation of high-energy fragmentation of hadrons and nuclei, as created experimentally in high-energy colliders, where a large number of interfering coupled channels limits robust classical simulation capabilities.

In this Appendix, the sign problem we have identified in Trotter evolution, which can be seen, for example, in Fig. 14(c), is dissected further in the system with $\Omega = N = 8$ modes, and for the set-4 couplings. The panels (a) and (b) of Fig. 21 show the sorted nonzero probability densities, $|\langle i|\psi\rangle|^2$ (with $|i\rangle$ being all the states in the computational basis, which, in base 10, are $\{0, \dots, 5^{\Omega/2} - 1\}$), associated with time-evolved states to $t = 0.4$, starting from $|\psi(0)\rangle_A$ and $|\psi(0)\rangle_B$. While they are somewhat different, as expected, the ranges of values are similar. The panels (c) and (d) show the sorted nonzero z -component spin densities, $\langle \psi|i\rangle\langle i|\hat{S}_z|\psi\rangle$, which are markedly different for the two initial states. There is a single large contribution when starting from $|\psi(0)\rangle_A$ that is not present when starting from $|\psi(0)\rangle_B$. The mean value and standard deviation of each element of $\langle \psi|i\rangle\langle i|\hat{S}_z|\psi\rangle$ are $\bar{x}_A = -0.03$ and $\sigma_A = 0.13$, providing an expectation value

of $\langle \hat{S}_z \rangle_A = -1.4$, and $\bar{x}_B = -0.004$ and $\sigma_B = 0.011$, giving $\langle \hat{S}_z \rangle_B = -0.17$.

Given that the range and magnitude of the probability densities in the wave function are comparable between the two initial condition, systematic errors introduced by Trotter evolution, or whatever algorithm is used for time evolution, and by the fidelity of the quantum device, in the probability distributions will be comparable. The same is true for the z -component spin density. However, the order-of-magnitude difference between the two spin densities, and particularly cancellations among contributions, means that spin densities from $|\psi(0)\rangle_B$ will be significantly more impacted than those from $|\psi(0)\rangle_A$ by time-evolution inaccuracies. The differing relative impacts of Trotter errors on the spin densities can be seen clearly in the lower panels in Fig. 21, in particular in the contrast between the lower-left (c) and lower-right (d) panels. This effect is responsible for the differing convergence of the spin density (and other observables) between $|\psi(0)\rangle_B$ and $|\psi(0)\rangle_A$ with decreasing Trotter step size that is seen in Fig. 14 and other such figures.

The behavior of Trotter errors in simulations starting from different initial states was previously considered in the context of complexity bounds [169–172]. It was found that the general error bounds can be improved for time evolution from states in the low-energy sector.

The identified sign problem is different in its nature to the StN problem in classical lattice QCD calculations at finite baryon number. There, the spectrum resulting from spontaneous breaking of the global chiral symmetries furnishes light pseudo-Goldstone bosons that contribute low-lying states to variance correlation functions associated with (multi)baryon correlation functions. In the present case, the cancellations between (small) amplitudes that produce small expectation values are disturbed by simulation errors, either systematic algorithm errors or device errors. Improving the StN problem at late times in baryon correlation functions determined with lattice QCD calculations requires exponentially large classical resources with increasing time. In contrast, the sign problem we have identified here originating from Trotterized time evolution can be systematically reduced by using smaller Trotter time intervals, which requires resources that scale with the

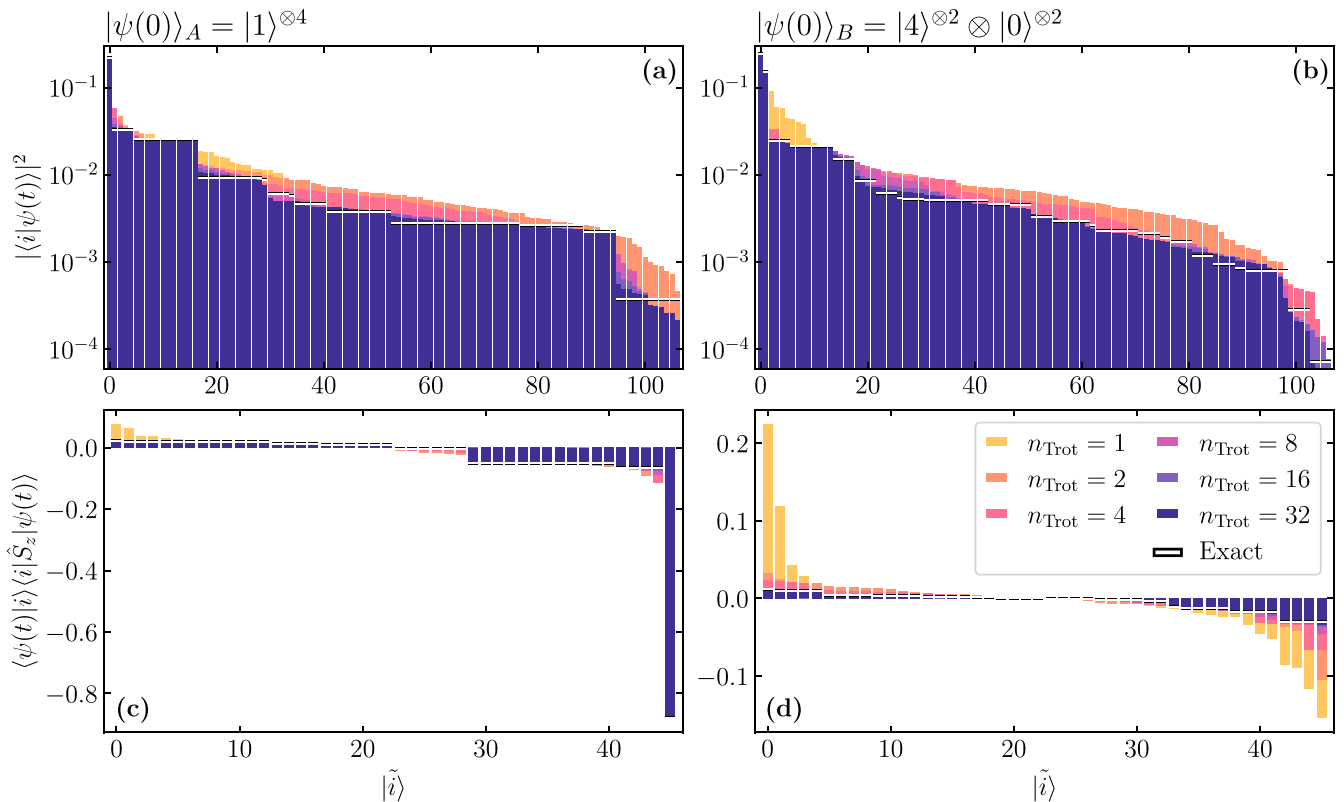


FIG. 21. (a), (b) Sorted nonzero values of probability density, $|\langle i|\psi\rangle|^2$, for each basis state in the wave function evolved to $t = 0.4$ with set-4 couplings (not all states $|i\rangle$ are shown, only those with non-zero contribution, labeled as $|\tilde{i}\rangle$). (c), (d) Sorted nonzero values of z component of spin density, $\langle\psi(t)|i\rangle\langle i|\hat{S}_z|\psi(t)\rangle$. The left panels (a), (c) correspond to the $|\psi(0)\rangle_A$ initial state, while the right panels (b), (d) correspond to the $|\psi(0)\rangle_B$ initial state.

number of Trotter steps. In the context of quantum simulations, this sign problem requires more extensive study to

estimate its impact on observables of interest, including the impact of transitions to chaotic evolution [173].

- [1] L. N. Cooper, Bound electron pairs in a degenerate Fermi gas, *Phys. Rev.* **104**, 1189 (1956).
- [2] J. Bardeen, L. N. Cooper, and J. R. Schrieffer, Microscopic theory of superconductivity, *Phys. Rev.* **106**, 162 (1957).
- [3] J. Bardeen, L. N. Cooper, and J. R. Schrieffer, Theory of superconductivity, *Phys. Rev.* **108**, 1175 (1957).
- [4] E. M. Nica and Q. Si, Multiorbital singlet pairing and d+d superconductivity, *npj Quantum Mater.* **6**, 3 (2021).
- [5] W. J. Holdhusen, S. Lerma-Hernández, J. Dukelsky, and G. Ortiz, Integrable model of topological SO(5) superfluidity, *Phys. Rev. B* **104**, L060503 (2021).
- [6] J. Dobrzyniecki, G. Orso, and T. Sowiński, Unconventional pairing in few-fermion systems tuned by external confinement, *Phys. Rev. Res.* **3**, 043105 (2021).
- [7] M. Bahari, S.-B. Zhang, C.-A. Li, S.-J. Choi, C. Timm, and B. Trauzettel, New type of helical topological superconducting pairing at finite excitation energies, [arXiv:2210.11955](https://arxiv.org/abs/2210.11955).
- [8] D. J. Dean and M. Hjorth-Jensen, Pairing in nuclear systems: From neutron stars to finite nuclei, *Rev. Mod. Phys.* **75**, 607 (2003).
- [9] M. G. Alford, A. Schmitt, K. Rajagopal, and T. Schäfer, Color superconductivity in dense quark matter, *Rev. Mod. Phys.* **80**, 1455 (2008).
- [10] C. V. Kraus, M. M. Wolf, J. I. Cirac, and G. Giedke, Pairing in fermionic systems: A quantum-information perspective, *Phys. Rev. A* **79**, 012306 (2009).
- [11] C. M. Ho and S. D. H. Hsu, Entanglement and fast quantum thermalization in heavy ion collisions, *Mod. Phys. Lett. A* **31**, 1650110 (2016).
- [12] D. E. Kharzeev and E. M. Levin, Deep inelastic scattering as a probe of entanglement, *Phys. Rev. D* **95**, 114008 (2017).
- [13] O. K. Baker and D. E. Kharzeev, Thermal radiation and entanglement in proton-proton collisions at energies available at the CERN Large Hadron Collider, *Phys. Rev. D* **98**, 054007 (2018).
- [14] S. R. Beane, D. B. Kaplan, N. Klco, and M. J. Savage, Entanglement suppression and emergent symmetries of strong interactions, *Phys. Rev. Lett.* **122**, 102001 (2019).
- [15] S. R. Beane and P. Ehlers, Chiral symmetry breaking entanglement and the nucleon spin decomposition, *Mod. Phys. Lett. A* **35**, 2050048 (2020).
- [16] Z. Tu, D. E. Kharzeev, and T. Ullrich, Einstein-Podolsky-Rosen paradox and quantum entanglement at subnucleonic scales, *Phys. Rev. Lett.* **124**, 062001 (2020).
- [17] S. R. Beane and R. C. Farrell, Geometry and entanglement in the scattering matrix, *Ann. Phys.* **433**, 168581 (2021).

- [18] G. Iskander, J. Pan, M. Tyler, C. Weber, and O. K. Baker, Quantum entanglement and thermal behavior in charged-current weak interactions, *Phys. Lett. B* **811**, 135948 (2020).
- [19] A. T. Kruppa, J. Kovács, P. Salamon, and Ö. Legeza, Entanglement and correlation in two-nucleon systems, *J. Phys. G* **48**, 025107 (2021).
- [20] S. R. Beane, R. C. Farrell, and M. Varma, Entanglement minimization in hadronic scattering with pions, *Int. J. Mod. Phys. A* **36**, 2150205 (2021).
- [21] N. Klco and M. J. Savage, Geometric quantum information structure in quantum fields and their lattice simulation, *Phys. Rev. D* **103**, 065007 (2021).
- [22] D. E. Kharzeev and E. Levin, Deep inelastic scattering as a probe of entanglement: Confronting experimental data, *Phys. Rev. D* **104**, L031503 (2021).
- [23] A. T. Kruppa, J. Kovács, P. Salamon, Ö. Legeza, and G. Zaránd, Entanglement and seniority, *Phys. Rev. C* **106**, 024303 (2022).
- [24] N. Klco, D. H. Beck, and M. J. Savage, Entanglement structures in quantum field theories: Negativity cores and bound entanglement in the vacuum, *Phys. Rev. A* **107**, 012415 (2023).
- [25] C. Robin, M. J. Savage, and N. Pillet, Entanglement rearrangement in self-consistent nuclear structure calculations, *Phys. Rev. C* **103**, 034325 (2021).
- [26] I. Low and T. Mehen, Symmetry from entanglement suppression, *Phys. Rev. D* **104**, 074014 (2021).
- [27] W. Gong, G. Parida, Z. Tu, and R. Venugopalan, Measurement of Bell-type inequalities and quantum entanglement from λ -hyperon spin correlations at high energy colliders, *Phys. Rev. D* **106**, L031501 (2022).
- [28] N. Klco, A. Roggero, and M. J. Savage, Standard model physics and the digital quantum revolution: thoughts about the interface, *Rep. Prog. Phys.* **85**, 064301 (2022).
- [29] C. W. Johnson and O. C. Gorton, Proton-neutron entanglement in the nuclear shell model, *J. Phys. G: Nucl. Part. Phys.* **50**, 045110 (2023).
- [30] D. Bai and Z. Ren, Entanglement generation in few-nucleon scattering, *Phys. Rev. C* **106**, 064005 (2022).
- [31] P. J. Ehlers, Entanglement between valence and sea quarks in hadrons of 1+1 dimensional QCD, *Ann. Phys. (NY)* **452**, 169290 (2023).
- [32] A. Tichai, S. Knecht, A. T. Kruppa, O. Legeza, C. P. Moca, A. Schwenk, M. A. Werner, and G. Zarand, Combining the in-medium similarity renormalization group with the density matrix renormalization group: Shell structure and information entropy, *Phys. Lett. B* **845**, 138139 (2023).
- [33] E. Pazy, The entanglement entropy between short range correlations and the Fermi sea in nuclear structure, *Phys. Rev. C* **107**, 054308 (2023).
- [34] A. Bulgac, Entanglement entropy, single-particle occupation probabilities, and short-range correlations, *Phys. Rev. C* **107**, L061602 (2023).
- [35] J. Faba, V. Martín, and L. Robledo, Analysis of quantum correlations within the ground state of a three-level Lipkin model, *Phys. Rev. A* **105**, 062449 (2022).
- [36] A. Bulgac, M. Kafker, and I. Abdurrahman, Measures of complexity and entanglement in many-fermion systems, *Phys. Rev. C* **107**, 044318 (2023).
- [37] M. A. Jafarizadeh, M. Ghapanvari, and N. Amiri, Entanglement entropy as a signature of a quantum phase transition in nuclei in the framework of the interacting boson model and interacting boson-fermion model, *Phys. Rev. C* **105**, 014307 (2022).
- [38] C. E. P. Robin and M. J. Savage, Quantum simulations in effective model spaces (I): Hamiltonian learning-VQE using digital quantum computers and application to the Lipkin-Meshkov-Glick model, *Phys. Rev. C* **108**, 024313 (2023).
- [39] C. Gu, Z. H. Sun, G. Hagen, and T. Papenbrock, Entanglement entropy of nuclear systems, *Phys. Rev. C* **108**, 054309 (2023).
- [40] Z. H. Sun, G. Hagen, and T. Papenbrock, Coupled-cluster theory for strong entanglement in nuclei, *Phys. Rev. C* **108**, 014307 (2023).
- [41] Z. Wang, X. Gu, L.-A. Wu, and Y.-X. Liu, Quantum simulation of pairing Hamiltonians with nearest-neighbor-interacting qubits, *Phys. Rev. A* **93**, 062301 (2016).
- [42] D. Lacroix, Symmetry assisted preparation of entangled many-body states on a quantum computer, *Phys. Rev. Lett.* **125**, 230502 (2020).
- [43] E. A. Ruiz Guzman and D. Lacroix, Accessing ground-state and excited-state energies in a many-body system after symmetry restoration using quantum computers, *Phys. Rev. C* **105**, 024324 (2022).
- [44] E. A. R. Guzman and D. Lacroix, Restoring broken symmetries using quantum search “oracles”, *Phys. Rev. C* **107**, 034310 (2023).
- [45] A. Khamoshi, F. A. Evangelista, and G. E. Scuseria, Correlating AGP on a quantum computer, *Quantum Sci. Technol.* **6**, 014004 (2021).
- [46] C. Jiang and J. Pei, Quantum computing of the pairing Hamiltonian at finite temperature, *Phys. Rev. C* **107**, 044308 (2023).
- [47] D. Agassi, Validity of the BCS and RPA approximations in the pairing-plus-monopole solvable model, *Nucl. Phys. A* **116**, 49 (1968).
- [48] H. Lipkin, N. Meshkov, and A. Glick, Validity of many-body approximation methods for a solvable model: (I). Exact solutions and perturbation theory, *Nucl. Phys.* **62**, 188 (1965).
- [49] J. Mumford and D. H. J. O’Dell, Critical exponents for an impurity in a bosonic Josephson junction: Position measurement as a phase transition, *Phys. Rev. A* **90**, 063617 (2014).
- [50] J. Vidal, G. Palacios, and C. Aslangul, Entanglement dynamics in the Lipkin-Meshkov-Glick model, *Phys. Rev. A* **70**, 062304 (2004).
- [51] M. Kitagawa and M. Ueda, Squeezed spin states, *Phys. Rev. A* **47**, 5138 (1993).
- [52] J. Ma, X. Wang, C. P. Sun, and F. Nori, Quantum spin squeezing, *Phys. Rep.* **509**, 89 (2011).
- [53] G. Salvatori, A. Mandarino, and M. G. A. Paris, Quantum metrology in Lipkin-Meshkov-Glick critical systems, *Phys. Rev. A* **90**, 022111 (2014).
- [54] L. Garbe, O. Abah, S. Felicetti, and R. Puebla, Critical quantum metrology with fully-connected models: From Heisenberg to Kibble-Zurek scaling, *Quantum Sci. Technol.* **7**, 035010 (2022).
- [55] J. Vidal, R. Mosseri, and J. Dukelsky, Entanglement in a first-order quantum phase transition, *Phys. Rev. A* **69**, 054101 (2004).
- [56] J. Vidal, G. Palacios, and R. Mosseri, Entanglement in a second-order quantum phase transition, *Phys. Rev. A* **69**, 022107 (2004).

- [57] J. I. Latorre, R. Orús, E. Rico, and J. Vidal, Entanglement entropy in the Lipkin-Meshkov-Glick model, *Phys. Rev. A* **71**, 064101 (2005).
- [58] H. T. Cui, Multiparticle entanglement in the Lipkin-Meshkov-Glick model, *Phys. Rev. A* **77**, 052105 (2008).
- [59] M. Di Tullio, R. Rossignoli, M. Cerezo, and N. Gigena, Fermionic entanglement in the Lipkin model, *Phys. Rev. A* **100**, 062104 (2019).
- [60] J. Faba, V. Martín, and L. Robledo, Two-orbital quantum discord in fermion systems, *Phys. Rev. A* **103**, 032426 (2021).
- [61] J. Faba, V. Martín, and L. Robledo, Correlation energy and quantum correlations in a solvable model, *Phys. Rev. A* **104**, 032428 (2021).
- [62] M. J. Cervia, A. B. Balantekin, S. N. Coppersmith, C. W. Johnson, P. J. Love, C. Poole, K. Robbins, and M. Saffman, Lipkin model on a quantum computer, *Phys. Rev. C* **104**, 024305 (2021).
- [63] A. Chikaoka and H. Liang, Quantum computing for the Lipkin model with unitary coupled cluster and structure learning ansatz, *Chin. Phys. C* **46**, 024106 (2022).
- [64] A. M. Romero, J. Engel, H. L. Tang, and S. E. Economou, Solving nuclear structure problems with the adaptive variational quantum algorithm, *Phys. Rev. C* **105**, 064317 (2022).
- [65] P. J. Ollitrault, A. Kandala, C.-F. Chen, P. K. Barkoutsos, A. Mezzacapo, M. Pistoia, S. Sheldon, S. Woerner, J. M. Gambetta, and I. Tavernelli, Quantum equation of motion for computing molecular excitation energies on a noisy quantum processor, *Phys. Rev. Res.* **2**, 043140 (2020).
- [66] M. Q. Hlatshwayo, Y. Zhang, H. Wibowo, R. LaRose, D. Lacroix, and E. Litvinova, Simulating excited states of the Lipkin model on a quantum computer, *Phys. Rev. C* **106**, 024319 (2022).
- [67] E. D. Davis and W. D. Heiss, Random-phase approximation and broken symmetry, *J. Phys. G: Nucl. Phys.* **12**, 805 (1986).
- [68] J. E. García-Ramos, J. Dukelsky, P. Pérez-Fernández, and J. M. Arias, Phase diagram of an extended Agassi model, *Phys. Rev. C* **97**, 054303 (2018).
- [69] A. Klein, T. Cohen, and C.-T. Li, Boson mappings for schematic nuclear models with the symmetry of $SO(5)$, *Ann. Phys. (NY)* **141**, 382 (1982).
- [70] P. Pérez-Fernández, J. M. Arias, J. E. García-Ramos, and L. Lamata, A digital quantum simulation of the Agassi model, *Phys. Lett. B* **829**, 137133 (2022).
- [71] A. Sáiz, J.-E. García-Ramos, J. M. Arias, L. Lamata, and P. Pérez-Fernández, Digital quantum simulation of an extended Agassi model: Using machine learning to disentangle its phase diagram, *Phys. Rev. C* **106**, 064322 (2022).
- [72] M. S. Alam *et al.*, Quantum computing hardware for HEP algorithms and sensing, [arXiv:2204.08605](https://arxiv.org/abs/2204.08605).
- [73] A. Romanenko, T. Kim, D. Frolov, R. Pilipenko, M. Reagor, S. Chakram, S. Belomestnykh, S. Zorzetti, S. Zhu, M. Bal, M. Checchin, D. van Zanten, A. Grassellino, and SQMS Team, Progress in the high coherence 3D SRF qubit architecture, in *APS March Meeting Abstracts*, APS Meeting Abstracts Vol. 2022 (APS, College Park, MD, 2022), p. Y34.008.
- [74] M. Neeley, M. Ansmann, R. C. Bialczak, M. Hofheinz, E. Lucero, A. D. O'Connell, D. Sank, H. Wang, J. Wenner, A. N. Cleland, M. R. Geller, and J. M. Martinis, Emulation of a quantum spin with a superconducting phase qudit, *Science* **325**, 722 (2009).
- [75] X. Tan, D.-W. Zhang, Q. Liu, G. Xue, H.-F. Yu, Y.-Q. Zhu, H. Yan, S.-L. Zhu, and Y. Yu, Topological maxwell metal bands in a superconducting qutrit, *Phys. Rev. Lett.* **120**, 130503 (2018).
- [76] M. Jerger, Y. Reshitnyk, M. Oppliger, A. Potočník, M. Mondal, A. Wallraff, K. Goodenough, S. Wehner, K. Juliusson, N. K. Langford, and A. Fedorov, Contextuality without nonlocality in a superconducting quantum system, *Nat. Commun.* **7**, 12930 (2016).
- [77] T. Liu, Q.-P. Su, J.-H. Yang, Y. Zhang, S.-J. Xiong, J.-M. Liu, and C.-P. Yang, Transferring arbitrary d -dimensional quantum states of a superconducting transmon qudit in circuit QED, *Sci. Rep.* **7**, 7039 (2017).
- [78] M. S. Blok, V. V. Ramasesh, T. Schuster, K. O'Brien, J. M. Kreikebaum, D. Dahlen, A. Morvan, B. Yoshida, N. Y. Yao, and I. Siddiqi, Quantum information scrambling on a superconducting qutrit processor, *Phys. Rev. X* **11**, 021010 (2021).
- [79] X. Wu, S. L. Tomarken, N. A. Petersson, L. A. Martinez, Y. J. Rosen, and J. L. DuBois, High-fidelity software-defined quantum logic on a superconducting qudit, *Phys. Rev. Lett.* **125**, 170502 (2020).
- [80] L. M. Seifert, Z. Li, T. Roy, D. I. Schuster, F. T. Chong, and J. M. Baker, Exploring ququart computation on a transmon using optimal control, [arXiv:2304.11159](https://arxiv.org/abs/2304.11159).
- [81] L. M. Seifert, J. Chadwick, A. Litteken, F. T. Chong, and J. M. Baker, Time-efficient qudit gates through incremental pulse re-seeding, [arXiv:2206.14975](https://arxiv.org/abs/2206.14975).
- [82] S. Choi, N. Y. Yao, and M. D. Lukin, Dynamical engineering of interactions in qudit ensembles, *Phys. Rev. Lett.* **119**, 183603 (2017).
- [83] M. F. O'Keeffe, L. Horesh, J. F. Barry, D. A. Braje, and I. L. Chuang, Hamiltonian engineering with constrained optimization for quantum sensing and control, *New J. Phys.* **21**, 023015 (2019).
- [84] H. Zhou, H. Gao, N. T. Leitao, O. Makarova, I. Cong, A. M. Douglas, L. S. Martin, and M. D. Lukin, Robust Hamiltonian engineering for interacting qudit systems, [arXiv:2305.09757](https://arxiv.org/abs/2305.09757).
- [85] P. J. Low, B. M. White, A. A. Cox, M. L. Day, and C. Senko, Practical trapped-ion protocols for universal qudit-based quantum computing, *Phys. Rev. Res.* **2**, 033128 (2020).
- [86] M. Ringbauer, M. Meth, L. Postler, R. Stricker, R. Blatt, P. Schindler, and T. Monz, A universal qudit quantum processor with trapped ions, *Nat. Phys.* **18**, 1053 (2022).
- [87] P. Hrmo, B. Wilhelm, L. Gerster, M. W. van Mourik, M. Huber, R. Blatt, P. Schindler, T. Monz, and M. Ringbauer, Native qudit entanglement in a trapped ion quantum processor, *Nat. Commun.* **14**, 2242 (2023).
- [88] K. Sun, C. Fang, M. Kang, Z. Zhang, P. Zhang, D. N. Beratan, K. R. Brown, and J. Kim, Quantum simulation of polarized light-induced electron transfer with a trapped-ion qutrit system, *J. Phys. Chem. Lett.* **14**, 6071 (2023).
- [89] A. Muthukrishnan and C. R. Stroud, Multivalued logic gates for quantum computation, *Phys. Rev. A* **62**, 052309 (2000).
- [90] S. S. Bullock, D. P. O'Leary, and G. K. Brennen, Asymptotically optimal quantum circuits for d -level systems, *Phys. Rev. Lett.* **94**, 230502 (2005).
- [91] T. C. Ralph, K. J. Resch, and A. Gilchrist, Efficient Toffoli gates using qudits, *Phys. Rev. A* **75**, 022313 (2007).
- [92] Z. Gedik, I. A. Silva, B. Çakmak, G. Karpat, E. L. G. Vidoto, D. O. Soares-Pinto, E. R. Deazevedo, and F. F. Fanchini, Computational speed-up with a single qudit, *Sci. Rep.* **5**, 14671 (2015).

- [93] P. Gokhale, J. M. Baker, C. Duckering, N. C. Brown, K. R. Brown, and F. T. Chong, Asymptotic improvements to quantum circuits via qutrits, in *Proceedings of the 46th International Symposium on Computer Architecture*, ISCA '19 (ACM Press, New York, 2019), pp. 554–566.
- [94] J. M. Baker, C. Duckering, and F. T. Chong, Efficient quantum circuit decompositions via intermediate qudits, in *Proceedings of the 2020 IEEE 50th International Symposium on Multiple-Valued Logic (ISMVL)* (IEEE Computer Society, Los Alamitos, CA, 2020), pp. 303–308.
- [95] D. Bruß and C. Macchiavello, Optimal eavesdropping in cryptography with three-dimensional quantum states, *Phys. Rev. Lett.* **88**, 127901 (2002).
- [96] N. J. Cerf, M. Bourennane, A. Karlsson, and N. Gisin, Security of quantum key distribution using d -level systems, *Phys. Rev. Lett.* **88**, 127902 (2002).
- [97] J. A. Gross, Designing codes around interactions: The case of a spin, *Phys. Rev. Lett.* **127**, 010504 (2021).
- [98] S. Lim, J. Liu, and A. Ardavan, Fault-tolerant qubit encoding using a spin-7/2 qudit, [arXiv:2303.02084](https://arxiv.org/abs/2303.02084).
- [99] S. Omanakuttan and J. A. Gross, Multispin Clifford codes for angular momentum errors in spin systems, *Phys. Rev. A* **108**, 022424 (2023).
- [100] A. Ciavarella, N. Klco, and M. J. Savage, Trailhead for quantum simulation of SU(3) Yang-Mills lattice gauge theory in the local multiplet basis, *Phys. Rev. D* **103**, 094501 (2021).
- [101] E. J. Gustafson, Prospects for simulating a qudit based model of (1+1)D scalar QED, *Phys. Rev. D* **103**, 114505 (2021).
- [102] E. Gustafson, Noise improvements in quantum simulations of sQED using qutrits, [arXiv:2201.04546](https://arxiv.org/abs/2201.04546).
- [103] D. González-Cuadra, T. V. Zache, J. Carrasco, B. Kraus, and P. Zoller, Hardware efficient quantum simulation of non-Abelian gauge theories with qudits on Rydberg platforms, *Phys. Rev. Lett.* **129**, 160501 (2022).
- [104] T. V. Zache, D. González-Cuadra, and P. Zoller, Fermion-qudit quantum processors for simulating lattice gauge theories with matter, *Quantum* **7**, 1140 (2023).
- [105] M. Calixto, A. Mayorgas, and J. Guerrero, Entanglement and $U(D)$ -spin squeezing in symmetric multi-quDit systems and applications to quantum phase transitions in Lipkin–Meshkov–Glick D -level atom models, *Quantum Inf. Process.* **20**, 304 (2021).
- [106] A. Klein and E. R. Marshalek, Boson realizations of lie algebras with applications to nuclear physics, *Rev. Mod. Phys.* **63**, 375 (1991).
- [107] K. D. Sviratcheva, A. I. Georgieva, V. G. Gueorguiev, J. P. Draayer, and M. I. Ivanov, Deformations of the fermion realization of the $sp(4)$ algebra and its subalgebras, *J. Phys. A* **34**, 8365 (2001).
- [108] K. D. Sviratcheva, J. P. Draayer, and A. I. Georgieva, An algebraic pairing model with $Sp(4)$ symmetry and its deformation, *J. Phys. G* **29**, 1281 (2003).
- [109] J. Dukelsky, V. G. Gueorguiev, P. Van Isacker, S. Dimitrova, B. Errea, and S. Lerma H., Exact solution of the isovector neutron-proton pairing Hamiltonian, *Phys. Rev. Lett.* **96**, 072503 (2006).
- [110] H. F. Trotter, On the product of semi-groups of operators, *Proc. Am. Math. Soc.* **10**, 545 (1959).
- [111] A. Peruzzo, J. McClean, P. Shadbolt, M.-H. Yung, X.-Q. Zhou, P. J. Love, A. Aspuru-Guzik, and J. L. O’Brien, A variational eigenvalue solver on a photonic quantum processor, *Nat. Commun.* **5**, 4213 (2014).
- [112] J. R. McClean, J. Romero, R. Babbush, and A. Aspuru-Guzik, The theory of variational hybrid quantum-classical algorithms, *New J. Phys.* **18**, 023023 (2016).
- [113] O. Higgott, D. Wang, and S. Brierley, Variational quantum computation of excited states, *Quantum* **3**, 156 (2019).
- [114] S. McArdle, T. Jones, S. Endo, Y. Li, S. C. Benjamin, and X. Yuan, Variational ansatz-based quantum simulation of imaginary time evolution, *npj Quantum Inf.* **5**, 75 (2019).
- [115] X. Yuan, S. Endo, Q. Zhao, Y. Li, and S. C. Benjamin, Theory of variational quantum simulation, *Quantum* **3**, 191 (2019).
- [116] H. R. Grimsley, S. E. Economou, E. Barnes, and N. J. Mayhall, An adaptive variational algorithm for exact molecular simulations on a quantum computer, *Nat. Commun.* **10**, 3007 (2019).
- [117] H. L. Tang, V. O. Shkolnikov, G. S. Barron, H. R. Grimsley, N. J. Mayhall, E. Barnes, and S. E. Economou, Qubit-ADAPT-VQE: An adaptive algorithm for constructing hardware-efficient *Ansätze* on a quantum processor, *PRX Quantum* **2**, 020310 (2021).
- [118] J. Stokes, J. Izaac, N. Killoran, and G. Carleo, Quantum natural gradient, *Quantum* **4**, 269 (2020).
- [119] B. Koczor and S. C. Benjamin, Quantum natural gradient generalized to noisy and nonunitary circuits, *Phys. Rev. A* **106**, 062416 (2022).
- [120] N. Gomes, A. Mukherjee, F. Zhang, T. Iadecola, C.-Z. Wang, K.-M. Ho, P. P. Orth, and Y.-X. Yao, Adaptive variational quantum imaginary time evolution approach for ground state preparation, *Adv. Quantum Technol.* **4**, 2100114 (2021).
- [121] N. Klco and M. J. Savage, Minimally entangled state preparation of localized wave functions on quantum computers, *Phys. Rev. A* **102**, 012612 (2020).
- [122] N. Goss, A. Morvan, B. Marinelli, B. K. Mitchell, L. B. Nguyen, R. K. Naik, L. Chen, C. Jünger, J. M. Kreikebaum, D. I. Santiago, J. J. Wallman, and I. Siddiqi, High-fidelity qutrit entangling gates for superconducting circuits, *Nat. Commun.* **13**, 7481 (2022).
- [123] L. E. Fischer, A. Chiesa, F. Tacchino, D. J. Egger, S. Carretta, and I. Tavernelli, Towards universal gate synthesis and error correction in transmon qudits, *PRX Quantum* **4**, 030327 (2023).
- [124] N. Klco and M. J. Savage, Systematically localizable operators for quantum simulations of quantum field theories, *Phys. Rev. A* **102**, 012619 (2020).
- [125] E. J. Heller, Bound-state eigenfunctions of classically chaotic Hamiltonian systems: Scars of periodic orbits, *Phys. Rev. Lett.* **53**, 1515 (1984).
- [126] Cirq developers, Cirq (2022) See full list of authors on Github: <https://github.com/quantumlib/Cirq/graphs/contributors>.
- [127] G. Van Rossum and F. L. Drake, *Python 3 Reference Manual* (CreateSpace, Scotts Valley, CA, 2009).
- [128] Quantum AI team and collaborators, qsim (2020).
- [129] A. Croy *et al.*, Expokit.jl: Julia implementations of Expokit, <https://github.com/acroy/Expokit.jl> (2018).
- [130] J. Bezanson, A. Edelman, S. Karpinski, and V. B. Shah, Julia: A fresh approach to numerical computing, *SIAM Rev.* **59**, 65 (2017).
- [131] M. Illa and M. J. Savage, Multi-neutrino entanglement and correlations in dense neutrino systems, *Phys. Rev. Lett.* **130**, 221003 (2023).

- [132] R. C. Farrell, I. A. Chernyshev, S. J. M. Powell, N. A. Zemlevskiy, M. Illa, and M. J. Savage, Preparations for quantum simulations of quantum chromodynamics in 1+1 dimensions. I. Axial gauge, *Phys. Rev. D* **107**, 054512 (2023).
- [133] R. S. Smith, M. J. Curtis, and W. J. Zeng, A practical quantum instruction set architecture, [arXiv:1608.03355](https://arxiv.org/abs/1608.03355).
- [134] D. S. Steiger, T. Häner, and M. Troyer, ProjectQ: An open source software framework for quantum computing, *Quantum* **2**, 49 (2018).
- [135] V. Gheorghiu, Quantum++: A modern c++ quantum computing library, *PLoS ONE* **13**, e0208073 (2018).
- [136] V. Bergholm *et al.*, PennyLane: Automatic differentiation of hybrid quantum-classical computations, [arXiv:1811.04968](https://arxiv.org/abs/1811.04968).
- [137] Z.-Y. Chen, Q. Zhou, C. Xue, X. Yang, G.-C. Guo, and G.-P. Guo, 64-qubit quantum circuit simulation, *Sci. Bull.* **63**, 964 (2018).
- [138] T. Jones, A. Brown, I. Bush, and S. C. Benjamin, QuEST and high performance simulation of quantum computers, *Sci. Rep.* **9**, 10736 (2019).
- [139] X.-C. Wu, S. Di, E. M. Dasgupta, F. Cappello, H. Finkel, Y. Alexeev, and F. T. Chong, Full-state quantum circuit simulation by using data compression, in *Proceedings of the International Conference for High Performance Computing, Networking, Storage and Analysis, SC '19* (ACM Press, New York, 2019).
- [140] S. Efthymiou, S. Ramos-Calderer, C. Bravo-Prieto, A. Pérez-Salinas, D. García-Martín, A. García-Saez, J. I. Latorre, and S. Carrazza, Qibo: A framework for quantum simulation with hardware acceleration, *Quantum Sci. Technol.* **7**, 015018 (2022).
- [141] G. G. Guerreschi, J. Hogaboam, F. Baruffa, and N. P. D. Sawaya, Intel quantum simulator: A cloud-ready high-performance simulator of quantum circuits, *Quantum Sci. Technol.* **5**, 034007 (2020).
- [142] X.-Z. Luo, J.-G. Liu, P. Zhang, and L. Wang, Yao.jl: Extensible, Efficient framework for quantum algorithm design, *Quantum* **4**, 341 (2020).
- [143] Y. Suzuki, Y. Kawase, Y. Masumura, Y. Hiraga, M. Nakadai, J. Chen, K. M. Nakanishi, K. Mitarai, R. Imai, S. Tamiya, T. Yamamoto, T. Yan, T. Kawakubo, Y. O. Nakagawa, Y. Ibe, Y. Zhang, H. Yamashita, H. Yoshimura, A. Hayashi, and K. Fujii, Qulacs: A fast and versatile quantum circuit simulator for research purpose, *Quantum* **5**, 559 (2021).
- [144] A. Li, B. Fong, C. Granade, G. Prawiroatmodjo, B. Heim, M. Roetteler, and S. Krishnamoorthy, SV-sim: Scalable PGAS-based state vector simulation of quantum circuits, in *Proceedings of the International Conference for High Performance Computing, Networking, Storage and Analysis, SC '21* (ACM Press, New York, NY, 2021).
- [145] L. Fang, ahehn-nv, hhbayraktar, and sam-stanwyck, NVIDIA/cuQuantum: cuQuantum Python v22.11.0.1 (2023).
- [146] T. F. Stetina, A. Ciavarella, X. Li, and N. Wiebe, Simulating effective QED on quantum computers, *Quantum* **6**, 622 (2022).
- [147] D. Janković, J.-G. Hartmann, M. Ruben, and P.-A. Hervieux, Noisy qudit vs multiple qubits: Conditions on gate efficiency, [arXiv:2302.04543](https://arxiv.org/abs/2302.04543).
- [148] D. Banerjee, M. Dalmonte, M. Muller, E. Rico, P. Stebler, U. J. Wiese, and P. Zoller, Atomic quantum simulation of dynamical gauge fields coupled to Fermionic matter: From string breaking to evolution after a quench, *Phys. Rev. Lett.* **109**, 175302 (2012).
- [149] B. Nachman, D. Provasoli, W. A. de Jong, and C. W. Bauer, Quantum algorithm for high energy physics simulations, *Phys. Rev. Lett.* **126**, 062001 (2021).
- [150] R. Verdel, F. Liu, S. Whitsitt, A. V. Gorshkov, and M. Heyl, Real-time dynamics of string breaking in quantum spin chains, *Phys. Rev. B* **102**, 014308 (2020).
- [151] A. Florio, D. Frenklakh, K. Ikeda, D. Kharzeev, V. Korepin, S. Shi, and K. Yu, Real-time non-perturbative dynamics of jet production: quantum entanglement and vacuum modification, *Phys. Rev. Lett.* **131**, 021902 (2023).
- [152] M. Illa, C. E. P. Robin, and M. J. Savage, https://github.com/millasub/Agassi_qu5it_data (2023).
- [153] <https://qscience.org>.
- [154] <https://hyak.uw.edu>.
- [155] <https://phys.washington.edu>.
- [156] <https://www.artsci.washington.edu>.
- [157] J. J. Wallman and J. Emerson, Noise tailoring for scalable quantum computation via randomized compiling, *Phys. Rev. A* **94**, 052325 (2016).
- [158] G. Parisi, The strategy for computing the hadronic mass spectrum, *Phys. Rep.* **103**, 203 (1984).
- [159] G. P. Lepage, From Actions to Answers, in *Proceedings of the 1989 Theoretical Advanced Study Institute in Elementary Particle Physics*, Boulder, CO, Report No. CLNS-89-971 (1989).
- [160] S. R. Beane, W. Detmold, T. C. Luu, K. Orginos, A. Parreño, M. J. Savage, A. Torok, and A. Walker-Loud (NPLQCD Collaboration), High statistics analysis using anisotropic clover lattices: I. Single hadron correlation functions, *Phys. Rev. D* **79**, 114502 (2009).
- [161] S. R. Beane, W. Detmold, T. C. Luu, K. Orginos, A. Parreño, M. J. Savage, A. Torok, and A. Walker-Loud (NPLQCD Collaboration), High statistics analysis using anisotropic clover lattices: II. Three-baryon systems, *Phys. Rev. D* **80**, 074501 (2009).
- [162] S. R. Beane, W. Detmold, H.-W. Lin, T. C. Luu, K. Orginos, M. J. Savage, A. Torok, and A. Walker-Loud (NPLQCD Collaboration), High statistics analysis using anisotropic clover lattices: III. Baryon-baryon interactions, *Phys. Rev. D* **81**, 054505 (2010).
- [163] M. G. Endres, D. B. Kaplan, J.-W. Lee, and A. N. Nicholson, Noise, sign problems, and statistics, *Phys. Rev. Lett.* **107**, 201601 (2011).
- [164] S. R. Beane, E. Chang, S. D. Cohen, W. Detmold, H. W. Lin, T. C. Luu, K. Orginos, A. Parreño, M. J. Savage, and A. Walker-Loud (NPLQCD Collaboration), Light nuclei and hypernuclei from quantum chromodynamics in the limit of SU(3) flavor symmetry, *Phys. Rev. D* **87**, 034506 (2013).
- [165] D. Grabowska, D. B. Kaplan, and A. N. Nicholson, Sign problems, noise, and chiral symmetry breaking in a QCD-like theory, *Phys. Rev. D* **87**, 014504 (2013).
- [166] S. R. Beane, W. Detmold, K. Orginos, and M. J. Savage, Uncertainty quantification in lattice QCD calculations for nuclear physics, *J. Phys. G* **42**, 034022 (2015).
- [167] M. L. Wagman and M. J. Savage, Statistics of baryon correlation functions in lattice QCD, *Phys. Rev. D* **96**, 114508 (2017).
- [168] M. L. Wagman and M. J. Savage, Taming the signal-to-noise problem in lattice QCD by phase reweighting, [arXiv:1704.07356](https://arxiv.org/abs/1704.07356).

- [169] B. Şahinoğlu and R. D. Somma, Hamiltonian simulation in the low-energy subspace, [npj Quantum Inf. 7, 119 \(2021\)](#).
- [170] Y. Su, H.-Y. Huang, and E. T. Campbell, Nearly tight Trotterization of interacting electrons, [Quantum 5, 495 \(2021\)](#).
- [171] D. An, D. Fang, and L. Lin, Time-dependent unbounded Hamiltonian simulation with vector norm scaling, [Quantum 5, 459 \(2021\)](#).
- [172] C. Yi and E. Crosson, Spectral analysis of product formulas for quantum simulation, [npj Quantum Inf. 8, 37 \(2022\)](#).
- [173] L. M. Sieberer, T. Olsacher, A. Elben, M. Heyl, P. Hauke, F. Haake, and P. Zoller, Digital quantum simulation, Trotter errors, and quantum chaos of the kicked top, [npj Quantum Inf. 5, 78 \(2019\)](#).